J Math Imaging Vis
DOI 10.1007/s10851-017-0728-2

Principal Curvature Measures Estimation and Application to 3D Face Recognition

Yinhang Tang[1] · **Huibin Li**[2] · **Xiang Sun**[3] · **Jean-Marie Morvan**[3,4] · **Liming Chen**[1]

Received: 4 August 2016 / Accepted: 27 March 2017

Abstract This paper presents an effective 3D face keypoint detection, description and matching framework based on three principle curvature measures. These measures give a unified definition of principle curvatures for both smooth and discrete surfaces. They can be reasonably computed based on the normal cycle theory and the geometric measure theory. The strong theoretical basis of these measures provides us a solid discrete estimation method on real 3D face scans represented as triangle meshes. Based on these estimated measures, the proposed method can automatically detect a set of sparse and discriminating 3D facial feature points. The local facial shape around each 3D feature point is comprehensively described by histograms of these principal curvature measures. To guarantee the pose invariance of these descriptors, three principle curvature vectors of these principle curvature measures are employed to assign the canonical directions. Similarity comparison between faces is accomplished by matching all these curvature-based local shape descriptors using the sparse representation-based reconstruction method. The proposed method was evaluated on three public databases, i.e. FRGC v2.0, Bosphorus, and Gavab. Experimental results demonstrated that the three principle curvature measures contain strong complementarity for 3D facial shape description, and their fusion can largely improve the recognition performance. Our approach achieves rank-one recognition rates of 99.6, 95.7, and 97.9% on the neutral subset, expression subset, and the whole FRGC v2.0 databases, respectively. This indicates that our method is robust to moderate facial expression variations. Moreover, it also achieves very competitive performance on the pose subset (over 98.6% except Yaw 90°) and the occlusion subset (98.4%) of the Bosphorus database. Even in the case of extreme pose variations like profiles, it also significantly outperforms the state-of-the-art approaches with a recognition rate of 57.1%. The experiments carried out on the Gavab databases further demonstrate the robustness of our method to varies head pose variations.

Keywords Principal curvature measures · 3D keypoint detection, description and matching · Expression, pose and occlusion · Mesh-based 3D face recognition

✉ Huibin Li
huibinli@mail.xjtu.edu.cn

Yinhang Tang
germain.tang-yinhang@doctorant.ec-lyon.fr

Xiang Sun
billy_sunxiang@hotmail.com

Jean-Marie Morvan
morvan@math.univ-lyon1.fr

Liming Chen
liming.chen@ec-lyon.fr

1 Université de Lyon, CNRS, Ecole Centrale de Lyon, LIRIS, 69134 Lyon, France

2 School of Mathematics and Statistics, Xi'an Jiaotong University, No.28, Xianning West Road, Xi'an, Shaanxi 710049, P.R. China

3 King Abdullah University of Science and Technologh, V.C.C. Research Center, Thuwal 23955-6900, Saudi Arabia

4 Université de Lyon, CNRS, Université Claude Bernard Lyon 1, ICJ UMR 5208, 69622 Villeurbanne, France

1 Introduction

Recently, with the rapid development of 3D imaging and visualization techniques, 3D shape analysis and processing (e.g. surface registration, 3D shape retrieval) have been widely studied. As stated in [57], capturing 3D shape makes an extremely wide array of new kinds of application possible.

Published online: 06 April 2017

For example, virtual reality (VR), augmented reality (AR), 3D biometrics, 3D human–machine interaction, 3D medical imaging, 3D remote sensing, to name just a few. Behind these applications, a fundamental and challenging problem is how to represent and characterize the geometric structures of these discrete 3D shapes (surfaces or volumes). Up to now, many approaches [9,12,60,65] have been proposed to solve this key issue.

As a special application of 3D shape analysis and processing, the key issue of 3D face recognition has also been widely addressed. Facial surface measurements, i.e. points [10], curves [63], stripes [5], regions [13,14], normals [39,77], curvatures [40,78], geodesic distance [11,42,43], have been popularly used to represent and characterize 3D face shapes. Among them, surface curvatures, including Gaussian curvature, mean curvature, principal curvatures, as well as shape index values, are the most widely used ones [16,20,28,39,40,42,43,67,76,78,84]. Thus, the representation and characterization of 3D face surface are the most important techniques for an efficient 3D face recognition system, where curvatures play fundamental effect.

However, 3D face scans are discrete surfaces and generally represented by discontinuous point clouds, depth images or piece-wise triangle meshes. This means that the classical curvature estimation formulations for at least C^2 smooth surfaces in the classical differential geometry are not suitable for 3D face scans. Instead of working directly on face scans, a popular solution is to estimate the curvatures of a polynomial surface patch achieved by fitting it to the local 3D facial surface. Otherwise, pointwise curvatures can also be estimated directly on triangle meshes. For example, the angle defect estimation [7] and the normal deviation estimation [85] are utilized to compute pointwise Gaussian curvature and mean curvature, respectively. However, the pointwise convergence guarantee is satisfied only for triangle meshes with special structure [86].

Fortunately, based on the normal cycle theory [17,58] and geometry measure theory [18,54], Morvan et al. proposed the concepts of generalized curvatures, i.e. curvature measures, for both smooth and discrete surfaces [17,54]. They further proposed a surface meshing algorithm and proved that Gaussian curvature measure and mean curvature measure of a triangle mesh converge to the ones of its sampled C^2 smooth surface, if the mesh is well-shaped (i.e. with minimal angle bound) and well-sized (i.e. with infinitesimal circumcircle) [41]. Recently, they further generalized the second fundamental form and asymptotic direction of smooth surface, and proposed asymptotic cone and principal curvature measures for general polyhedral surface [73]. The convergence of the principal curvature measures can also be guaranteed based on the normal cycle theory [73] (see Sect. 3 for more details).

Motivated by this curvature estimation method for triangle meshes, a natural idea is to see how these generalized curvatures (i.e. principal curvature measures) can be used for 3D face recognition? How to estimate them on meshed 3D face scans, and are they effective and efficient for 3D face description and recognition? To answer these questions, we give the following **contributions** in this paper:

1. Different from all the existing 3D face recognition approaches, we are the first attempting to study the effectiveness of the principal curvature measures for the practical 3D face recognition application.
2. We improved our previous work [78] and designed novel 3D facial keypoint detection and description schemes based on principal curvature measures, and their corresponding principal curvature vectors.
3. We conducted comprehensive experiments on three 3D face databases, i.e., FRGC v2.0, Bosphorus and Gavab, to evaluate the general face recognition performance and the robustness to pose and occlusion variations of the proposed approach.

Specifically, the proposed 3D face recognition approach consists of three modules. First of all, a group of discriminating feature points are detected automatically based on principal curvature measures. Then, the histograms of three principal curvature measures describe comprehensively the local shape around these feature points. The descriptor is further endowed with rotation invariance by assigning canonical direction based on the corresponding principal curvature vectors. The similarity measurement between face scans is finally defined as the sparse representation-based reconstruction error.

The proposed method was comprehensively evaluated on three public 3D face databases, i.e. FRGC v2.0 [59], Bosphorus [64], and Gavab [53]. On the FRGC v2.0 databases, the effectiveness of each single curvature-based descriptor is validated, and the discriminative power of their score-level fusion demonstrates the strong informative complementarity among different principal curvature measures. Our approach achieves rank-one recognition rates of 99.6% with neutral probes and 95.7% with expressive probes, and a verification rate of 95.28% with 0.1% false accept rate (FAR). Moreover, when the experiments performed on the pose subsets of the Bosphorus and the Gavab databases, the proposed approach achieves the best scores among the state-of-the-art ones showing its robustness to diverse pose changes. The outstanding recognition results of the descriptors are also presented when different external occlusions are involved.

The rest of this paper is organized as follows. Section 2 gives a brief review of related works on 3D face recognition and curvature estimation on discrete surfaces. Section 3 introduces the theory of principal curvature measures of smooth surface, triangle mesh, as well as the meshed 3D facial surface. 3D face recognition method based on prin-

cipal curvature measures and their corresponding principal curvature vectors is introduced in Sect. 4. Section 5 reports the experimental results, and Sect. 6 finally concludes the paper.

2 Related Work

As aforementioned, the characterization and description of 3D face scans based on geometric attributes are the key parts for 3D face recognition, in which curvatures play an important role. In general, there are two common categories of curvature estimation methods on triangle mesh: *discrete* and *continuous* ones [61,74]. The *discrete* methods estimate curvatures with a closed-form differential geometry operators and work directly on triangle mesh. For example, Meyer et al. [50] proposed to use the average Voronoi cells and mixed finite element/finite volume method to formulate the first- and second-order differential operators. Taubin [79] proposed to compute principal curvatures and principal directions from a 3×3 symmetric matrices defined by integral formulas relating to a curvature tensor. While *continuous* methods prefer to fit a smooth surface patch using the points on the discrete triangle mesh and estimate curvatures on the approximated smooth surface. Hamann [32] proposed to fit a quadratic surface for curvature estimation. Goldfeather et al. [27] used a cubic-order local surface fitting method to estimate principal curvatures and principal directions. Theisel et al. [80] proposed to estimate curvature tensor through normal vector of each triangle facet. Rusinkiewicz [62] used the robust statistics, i.e. M-estimation, to estimate both curvatures and their derivatives based on normal vectors. All these methods estimate pointwise curvatures, and the convergence results of these methods depend largely on the mesh quality or the local smooth surfaces used for fitting.

A different view of defining curvatures on discrete surfaces is using the concept of "curvature measure", which is developed in [17] based on the normal cycle theory and geometry measure theory. Given well-sized and well-shaped triangle meshes sampled from C^2 smooth surfaces, the convergence of curvature measures can be guaranteed, and the approximation errors can also be well estimated [41,54]. Recently, Sun and Morvan generalized the second fundamental form and asymptotic direction of smooth surface and proposed the concepts of asymptotic cone for general polyhedral surface [73]. Benefiting from their approach, the curvature measures associated to a neighbourhood region around a point can be estimated correctly and directly on the triangle mesh (see Sect. 3). In this paper, we will introduce these generalized curvatures into the 3D face recognition application.

According to [38], 3D face recognition approaches can be generally classified into three categories. That is *local region/feature* based [1,25,33,82], *surface-distance* based [10,23,63], and *expression deformation modelling* based [37,46,56]. In this paper, we only summarize some very related 3D face recognition approaches in which curvatures are used for face description. Please refer to [8,38,66] for a comprehensive survey of 3D face recognition.

In 1992, Gordon [28] proposed to use principal curvatures to extract rigid facial regions, and curvature maps to detect facial features. This is perhaps the first curvature-based 3D face recognition method. Tanaka et al. [76] used Extended Gaussian Image (EGI) of facial rigid and valley lines for face representation. Wu et al. [84] adopted the minimum curvature for salient points detection. Li et al. [42,43] built a low-level geometric feature pool, including Gaussian curvature and mean curvature, for 3D face representation and recognition. Szeptycki et al. [75] introduced a coarse-to-fine 3D face landmarking solution based on the facial curvature analysis and a generic 3D face model. Chang et al. [14] proposed a curvature-based facial surface segmentation method for 3D+2D face recognition. Mian et al. [51] presented the Spherical Face Representation for 3D face recognition, and employed principal curvatures to check the position of salient facial points. Lu et al. [47] used shape index (i.e. curvatures) for facial keypoint detection. Smeets et al. [67] proposed a general 3D facial keypoint detection, description and matching framework for 3D face recognition, in which the mean curvature is used for keypoint detection, shape index and slant angle are employed for keypoint description. Li et al. [40] generalized all the three components of the framework of [67] and developed an expression, pose and occlusion robust 3D face recognition method. In particular, they proposed to use both the maximum and minimum curvatures for facial keypoint detection, and multiple-order surface differential quantities (normal, shape index, the derivative of shape index) for facial keypoint description. To the best of our knowledge, this is one of the most robust and efficient framework which computes the distribution of curvatures and makes curvatures be a very discriminative facial surface descriptor in the literature of 3D face recognition. In this paper, we will also use this general framework for 3D face recognition. However, in contrast to the local patch fitting-based curvature estimation methods [40,42,43,87], we are the first attempting to study the usability and effectiveness of the principal curvature measures for 3D face description and recognition.

3 Principal Curvature Measures: Background, Definition and Estimation

In this section, we first review the background on currents, the concept of normal cycle and the classical pointwise *second fundamental form*, *principal curvatures* and *principal vector fields* of smooth surfaces embedded in $\mathbb{R}^3$. We then define

the curvature measures in a general setting and in the special case of triangle meshes, that is, the triangle meshes adapted to 3D face recognition problem.

3.1 Background on Currents

We denote by $\mathbb{R}^n$ the n-dimensional $\mathbb{R}$-vector space, endowed with its standard scalar product $< .,. >$. Details on basic definitions and properties on *differential forms* defined on $\mathbb{R}^n$ or a submanifold of $\mathbb{R}^n$ can be found in [68,69].

3.1.1 General Currents

We denote by $\mathcal{D}^m(\mathbb{R}^n)$ the $\mathbb{R}$-vector space of smooth *differential m-forms* with compact support on $\mathbb{R}^n$. It is endowed with the topology of the uniform convergence on any compact subset of all partial derivatives of any order. We denote by $\mathcal{D}_m(\mathbb{R}^n)$ the space of *m-currents* of $\mathbb{R}^n$, that is, the topological dual of $\mathcal{D}^m(\mathbb{R}^n)$. The duality bracket will also be denoted by $< \cdot, \cdot >$. The *support* $spt(T)$ of a m-current T of $\mathbb{R}^n$ is the smallest closed subset $C \subset \mathbb{R}^n$ such that, if $\omega \in \mathcal{D}^m(\mathbb{R}^n)$ satisfies $spt(\omega) \cap C = \emptyset$, then $< T, \omega >= 0$. We endow $\mathcal{D}_m(TM^N)$ with the weak topology : if $(T_k)_{k\in\mathbb{N}}$ is a sequence of m-currents of $\mathbb{R}^n$ and if T is a m-current of $\mathbb{R}^n$, then

$$\lim_{k\to\infty} T_k = T \iff \forall \omega \in \mathcal{D}^m(\mathbb{R}^n) \quad \lim_{k\to\infty} < T_k, \omega >=< T, \omega > . \tag{1}$$

The *boundary* of a m-current T is the $m-1$ current ∂T defined for every $\varphi \in \mathcal{D}^{m-1}(\mathbb{R}^n)$ by

$$< \partial T, \varphi >=< T, d\varphi > . \tag{2}$$

A current T is *closed* if $\partial T = 0$.

3.1.2 Rectifiable Currents

The link between *currents* and *measures* can be done as follows: we denote by $\mathcal{H}^m$ the Hausdorff measure on $\mathbb{R}^n$. A subset $\mathcal{A}$ of $\mathbb{R}^n$ is *m-rectifiable* if its $\mathcal{H}^m$-measure is finite, and if almost all of $\mathcal{A}$ (for the $\mathcal{H}^m$-measure) is included in the union of the images of a countably set of Lipschitz functions from $\mathbb{R}^m$ to $\mathbb{R}^n$. It is well known that if $\mathcal{A}$ is m-rectifiable, it admits a m-dimensional tangent vector space $T_p\mathcal{A}$ at $\mathcal{H}^m$-almost every point $p \in \mathcal{A}$. An *orientation* of a *m-rectifiable* subset $\mathcal{A}$ of $\mathbb{R}^n$ is the choice of a $\mathcal{H}^m$-measurable orientation defined at each tangent subspace $T_p\mathcal{A}$. For example, given for instance by an (oriented) basis $(v_1, v_2, \ldots, v_m)_p$ of $T_p\mathcal{A}$, or given by the corresponding m-vector $v_p = (v_1 \wedge \ldots \wedge v_m)_p$, or by the m-form $(\theta^1 \wedge \ldots \wedge \theta^m)_p$, where $(\theta^1, \ldots, \theta^m)_p$ is the basis dual to the basis $(v_1, \ldots, v_m)_p$. Roughly speaking, an (oriented) m-rectifiable subset of $\mathbb{R}^n$ can be intuitively interpreted as a "smooth m-dimensional (oriented) sub-manifolds with singularities". A m-current T (with compact support) in $\mathbb{R}^n$ is *rectifiable* if there exists a m-rectifiable subset $\mathcal{A}$ endowed with an orientation v, an integrable function c with positive integer values defined at each point of $\mathcal{A}$ admitting a tangent vector space, satisfying $\int_{\mathcal{A}} c\mathcal{H}^m < \infty$, and such that, for every m-differential form with compact support ω,

$$< T, \omega >= \int_{\mathcal{A}} < v, \omega > c\mathcal{H}^n. \tag{3}$$

Details can be found for instance in [54].

If B is any measurable set, the restriction of T to B is defined as follows :

$$< T \llcorner B, \varphi >= \int_{\mathcal{A}} < v, \omega > c\chi_B \mathcal{H}^n. \tag{4}$$

where χ_B is the characteristic function of B. A m-current is *integral* if it is rectifiable and its boundary is rectifiable.

3.2 The Normal Cycle

Let $T\mathbb{R}^3$ denotes the tangent bundle of $\mathbb{R}^3$, identified to $\mathbb{R}^3 \times \mathbb{R}^3$. The unit tangent bundle $ST\mathbb{R}^3 \subset T\mathbb{R}^3$ of $\mathbb{R}^3$ can then be identified to $\mathbb{R}^3 \times \mathbb{S}^2$, where $\mathbb{S}^2$ denotes the unit sphere of $\mathbb{R}^3$. When it exists, the *normal cycle* associated to a (compact singular) subset $\mathcal{W}$ of $\mathbb{R}^3$ is a closed integral 2-current $\mathbf{N}(\mathcal{W}) \in \mathcal{D}_2(T\mathbb{R}^3) = \mathcal{D}_2(\mathbb{R}^6)$. It is the direct generalization of the unit normal bundle of a smooth surface of $\mathbb{R}^3$. A formal definition has been given in [26]. This normal cycle can be defined for a large class of compact subsets, as convex subsets and polyhedra, in particular for triangle meshes. (But up to now, one does not know if this definition can be extended to associate a normal cycle to *any* compact subset of $\mathbb{R}^6$.) A compact subset $\mathcal{G}$ of $\mathbb{R}^3$ such that $\mathbf{N}(\mathcal{G})$ exists is said to be *geometric*, and $\mathbf{N}(\mathcal{G})$ is called its *normal cycle*. The main property of the normal cycle is its additivity [26]:

Proposition 1 *If $\mathcal{G}_1$ and $\mathcal{G}_2$ are geometric, then $\mathcal{G}_1 \cup \mathcal{G}_2$ and $\mathcal{G}_1 \cap \mathcal{G}_2$ are geometric and*

$$\mathbf{N}(\mathcal{G}_1 \cup \mathcal{G}_2) = \mathbf{N}(\mathcal{G}_1) + \mathbf{N}(\mathcal{G}_2) - \mathbf{N}(\mathcal{G}_1 \cap \mathcal{G}_2). \tag{5}$$

This inclusion–exclusion formula allows to compute explicitly the normal cycle of a geometric set $\mathcal{G}$ by decomposing the $\mathcal{G}$ in suitable simple subsets and computing the normal cycle of each subset. Figure 1 shows the example of the additivity of the normal cycle. The basic examples of normal cycles are the following ones :

1. If D is a compact domain whose boundary is a smooth (oriented) surface S of $\mathbb{R}^3$, then its normal cycle is the

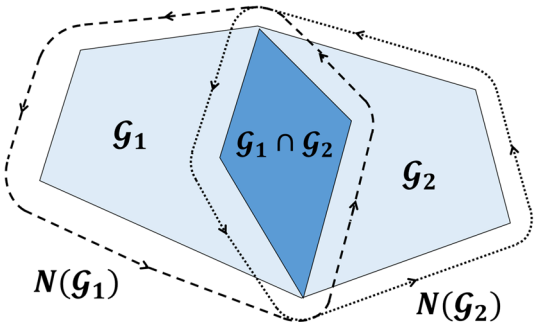

Fig. 1 For instance, in the simple situation of two (plain) polygons $\mathcal{G}_1$ and $\mathcal{G}_2$ in the plane $\mathbb{R}^2$, the normal cycle of $\mathcal{G}_1 \cup \mathcal{G}_2$ can be calculated using formula (5) by computing the normal cycle of $\mathcal{G}_1$ (resp. $\mathcal{G}_1$, resp. $\mathcal{G}_1 \cap \mathcal{G}_2$). In this figure, the normal cycles are represented by the *oriented dot lines*. These *dot lines* are the images in $\mathbb{R}^2$ of the normal cycles by the map $\phi : \mathbb{R}^2 \times \mathbb{R}^2 \to \mathbb{R}^2$ given by $\phi(p, \xi) = p + \xi$

closed current associated to its unit oriented normal bundle. (If there is no possible confusion, it is denoted by $\mathbf{N}(S)$ instead of $\mathbf{N}(D)$.)

2. If C is a convex body, then its normal cycle is the closed current associated to the oriented set $\{(m, \xi) \ : \ m \in \partial C, \xi \in \mathbb{R}^3, ||\xi|| = 1, \forall z \in C, < \xi, \overrightarrow{mz} > \leq 0\}$.
3. The normal cycle of a (compact) domain $\mathcal{W}$ of $\mathbb{R}^3$ whose boundary is a polyhedron $\mathcal{P}$ can be computed by applying (5) to a decomposition of $\mathcal{W}$ into (convex) simplicities, and using the previous sample. (If there is no possible confusion, it is also denoted by $\mathbf{N}(\mathcal{P})$ instead of $\mathbf{N}(\mathcal{W})$.)

3.3 Curvature Functions, Curvature Measures for Smooth Surfaces

In this section, we first review the classical pointwise *second fundamental form*, *principal curvatures*, *principal vector fields*, of smooth surfaces S embedded in $\mathbb{R}^3$. We introduce the concept of *second fundamental measure* and *principal curvature measures* for such smooth surfaces. For simplicity, we can assume that S bounds a compact domain D (and then has no boundary). This classical background can be found in [15,22,54] for instance.

3.3.1 Classical Principal Curvatures of Smooth Surfaces in $\mathbb{R}^3$

Let us consider a smooth oriented surface S embedded in the Euclidean space $\mathbb{R}^3$. Let ξ be a normal vector field, h the second fundamental form of S in the normal direction ξ. At each point p of S, the eigenvalues of h_p are called the *principal curvatures* $\lambda_{1p}, \lambda_{2p}$ of S. The eigenvectors of h_p (tangent to S) are called the *principal curvature vectors* e_{1p}, e_{2p} at p. In an orthonormal frame of eigenvectors (e_{1p}, e_{2p}) at p, the matrix of h_p is

$$\begin{pmatrix} \lambda_{1_p} & 0 \\ 0 & \lambda_{2_p} \end{pmatrix}.$$

The local bending informations (around any point p) of S can be described by its second fundamental form, in particular by its principal curvatures and principal directions.

One remarks that the previous constructions and definitions make sense because of the smoothness of S : Indeed, to define h, one needs to differentiate twice a parametrisation of S. To describe the local bending information of triangle meshes, one must generalize these constructions to non-smooth objects. A possible solution is to replace functions by measures. It is the goal of Sect. 3.3.2 in the smooth surface case: we will associate a measure to h, and in Sect. 3.5, we will define the corresponding measure for any triangle mesh.

3.3.2 Second Fundamental Measures of Smooth Surfaces in $\mathbb{R}^3$

Let S be a smooth surface (to simplify, we can assume that it bounds a compact domain, and we denote by ξ the outward normal vector field). To any Borel subset B of $\mathbb{R}^3$ and any vector field X and Y of $\mathbb{R}^3$, we define

$$\overline{h}^S_B(X, Y) = \int_{S \cap B} h_p(pr_{T_pS} X_p, pr_{T_pS} Y_p) dp, \tag{6}$$

where pr_{T_pS} denotes the orthogonal projection over the tangent plane T_pS of S at p. For fixed X and Y, the map

$$B \to \overline{h}^S_B(X, Y) \tag{7}$$

is a signed measure on $\mathbb{R}^3$. Moreover, if we restrict the set of vector fields X and Y in $\mathbb{R}^3$ to *constant* vector fields in $\mathbb{R}^3$, then for any fixed Borel subset B of $\mathbb{R}^3$, the map :

$$\begin{array}{rl} \mathbb{R}^3 \times \mathbb{R}^3 \to & \mathbb{R}, \\ (X, Y) \ \to & \overline{h}^S_B(X, Y) \end{array} \tag{8}$$

is a symmetric bilinear form on $\mathbb{R}^3$. Let $(\lambda^S_{1_B}, \lambda^S_{2_B}, \lambda^S_{3_B})$ denotes its three eigenvalues and $(e_{1_B}, e_{2_B}, e_{3_B})$ the corresponding eigenvectors. For every $i \in \{1, 2, 3\}$, the map

$$\lambda_i : B \to \lambda^S_{i_B} \tag{9}$$

is a *measure* on $\mathbb{R}^3$ called the ith *principal curvature measure*. In the same way, the eigenvectors of $\overline{h}^S_B$ are called the *principal curvature vectors* of S over B. Remark that we now get three principal curvatures instead of two in the pointwise approach. In the orthonormal frame of principal vectors, the matrix of $\overline{h}^S_B$ is now

$$\begin{pmatrix} \lambda^S_{1_B} & 0 & 0 \\ 0 & \lambda^S_{2_B} & 0 \\ 0 & 0 & \lambda^S_{3_B} \end{pmatrix}. \tag{10}$$

Moreover, let us remark that if we suppose that the Borel subset B is reduced to a point $p \in S$, and $y_p \in T_pS$, $\overline{h}(p)$ can be considered as a Dirac measure, with $\overline{h}^y_S(\{p\}) = h_p(y_p, y_p)$, where T_pS denotes the tangent plane of S at p. If $z_p = \xi_p$, where ξ_p denotes the normal vector of p, then $\overline{h}^z_S(\{p\}) = 0$. Then, in the frame of $(e_{1_p}, e_{2_p}, \xi_p)$ the matrix of $\overline{h}(p)$ becomes

$$\begin{pmatrix} \lambda^S_{1_p} & 0 & 0 \\ 0 & \lambda^S_{2_p} & 0 \\ 0 & 0 & 0 \end{pmatrix}.$$

As mentioned in [18,54,73], because our purpose will apply principal curvature measures on triangle meshes for 3D face recognition, it appears useful to introduce a slightly different measure : We define

$$\overline{h}^S_B(X, Y) = \int_{S\cap B} h_p(j \circ pr_{T_pS} X_p, j \circ pr_{T_pS} Y_p) dp, \tag{11}$$

where, at each point p, j is the direct rotation of angle $\frac{\pi}{2}$ in the tangent plane T_pS. Consequently, at each point p, one must swap the eigenvalues in the tangent plane, that is, replace the matrix in (10) by the matrix

$$\begin{pmatrix} \lambda^S_{2_B} & 0 & 0 \\ 0 & \lambda^S_{1_B} & 0 \\ 0 & 0 & \lambda^S_{3_B} \end{pmatrix}.$$

The theoretical approach is exactly the same and the computations are simpler.

3.4 Curvature Measures for Singular Spaces

The goal of this section is to define a framework that gives the possibility to define *curvature measures* for a large class of singular objects, namely geometric subsets of $\mathbb{R}^3$ (in our context), and that generalizes the curvature measures defined in Sect. 3.3.2 for smooth objects. The idea is to define such measures by means of a differential forms on the unit tangent bundle of $\mathbb{R}^3$.

We denote by $ST\mathbb{R}^3 \subset T\mathbb{R}^3$ the bundle of unit tangent vectors of $\mathbb{R}^3$ (identified to $\mathbb{R}^3 \times \mathbb{S}^2$), where $\mathbb{S}^2$ denotes the unit sphere of $\mathbb{R}^3$. For every vector fields X and Y on $\mathbb{R}^3$, the *second fundamental curvature form* is the 2-differential form $\omega^{X,Y}$ on $ST\mathbb{R}^3$ defined as follows : at each point $(m, \xi) \in ST\mathbb{R}^3$,

$$\omega^{X,Y}_{m,\xi} = X \wedge (\xi \times Y),$$

where $\times$ denotes the vector product in $\mathbb{R}^3$. In this formula, we have identified vectors and 1-form using the duality defined by the scalar product of $\mathbb{R}^3$. We can now define the *second fundamental curvature measure* of any geometric set :

Definition 1 Let $\mathcal{G}$ be a geometric subset of $\mathbb{R}^3$. The second fundamental vector valued measure $\Phi_\mathcal{G}$ of $\mathcal{G}$ is defined as follows : For any vector fields X and Y on $\mathbb{R}^3$,

$$\forall B \in \mathcal{B}_{\mathbb{R}^3}, \Phi^{X,Y}_\mathcal{G}(B) = \mathbf{N}(\mathcal{G})\llcorner(B \times \mathbb{R}^3)\omega^{X,Y}. \tag{12}$$

The crucial point is the following result [17,18]:

Theorem 1 *If $\mathcal{G}$ is a smooth surface, then $\Phi_\mathcal{G} = \overline{h}^\mathcal{G}$.*

This theorem claims that if the geometric set $\mathcal{G}$ is a smooth surface, then $\Phi_\mathcal{G}$ is nothing but "the integral of $\overline{h}$ over $\mathcal{G}$". Thus, $\Phi_\mathcal{G}$ is a "good" generalisation of $\overline{h}$. Mimicking Sect. 3.3.2, we now restrict the set of vector fields X, Y in $\mathbb{R}^3$ to *constant* vector fields. Then, for any fixed Borel subset B of $\mathbb{R}^3$, the map :

$$\begin{array}{rcl} \mathbb{R}^3 \times \mathbb{R}^3 \to & \mathbb{R}, \\ (X, Y) & \to \Phi^{X,Y}_\mathcal{G}(B) \end{array} \tag{13}$$

is a bilinear symmetric form on $\mathbb{R}^3$. Let us denote by $(\lambda^\mathcal{G}_{1_B}, \lambda^\mathcal{G}_{2_B}, \lambda^\mathcal{G}_{3_B})$ its three eigenvalues. For every $i \in \{1, 2, 3\}$, the map

$$\lambda^\mathcal{G}_i : B \to \lambda^\mathcal{G}_{i_B} \tag{14}$$

is again a *measure* on $\mathbb{R}^3$ called the ith *principal curvature measure* of $\mathcal{G}$ over B. In the same way, the corresponding eigenvectors are called the *principal curvature vectors* of $\mathcal{G}$ over B. In the orthonormal frame of principal vectors, the corresponding matrix is

$$\begin{pmatrix} \lambda^\mathcal{G}_{1_B} & 0 & 0 \\ 0 & \lambda^\mathcal{G}_{2_B} & 0 \\ 0 & 0 & \lambda^\mathcal{G}_{3_B} \end{pmatrix}. \tag{15}$$

3.5 Principal Curvature Measures of Triangle Meshes in $\mathbb{R}^3$

We now deal with triangular meshes $\mathcal{T}$ in $\mathbb{R}^3$. For simplicity, as for smooth surfaces, we assume that $\mathcal{T}$ bounds a compact domain. Since a triangular mesh is a singular surface, one cannot describe its shape by using a pointwise approach. That is why we will use the measure theoretic approach described in Sect. 3.4. We denote by E the set of edges e of $\mathcal{T}$, $l(e \cap B)$ the length of $e \cap B$, and $\angle(e)$ the signed angle between the unit oriented normal n_1 of face f_1 (*resp.* n_2 of face f_2) incident to e (The sign is determined as follows: if the angle of the

oriented normals of f_1 and f_2 pointing inside the domain is less or equal to π, the sign is positive. It is negative in the other case.). For any Borel subset B of $\mathbb{R}^3$, and any constant vector fields X and Y in $\mathbb{R}^3$, we deduce from (12) by a direct computation the following explicit formula :

$$\Phi_{\mathcal{T}}^{X,Y}(B) = \sum_{e \in E} l(e \cap B) \angle(e) < X, e >< Y, e > . \tag{16}$$

In other words, in any fixed frame, the matrix $M_B^{\mathcal{T}}$ associated to $\overline{h}_B$ satisfies :

$$M_B^{\mathcal{T}} = \sum_{e \in E} l(e \cap B) \angle(e) e \cdot e^t. \tag{17}$$

A classical explicit diagonalization of $M_B^{\mathcal{T}}$ gives the three principal curvature measures of B and the corresponding diagonalised matrix

$$\begin{pmatrix} \lambda_{1_B}^{\mathcal{T}} & 0 & 0 \\ 0 & \lambda_{2_B}^{\mathcal{T}} & 0 \\ 0 & 0 & \lambda_{3_B}^{\mathcal{T}} \end{pmatrix}. \tag{18}$$

Similarly to the smooth case, the set of eigenvalues $(\lambda_{1_B}, \lambda_{2_B}, \lambda_{3_B})$ of $\overline{h}_B$ are called the *principal curvature measures* of $\mathcal{T}$ over B and the eigenvectors $(e_{1_B}, e_{2_B}, e_{3_B})$ of $\overline{h}_B$ are called the *principal curvature vectors* of $\mathcal{T}$ over B.

3.6 A Convergence Theorem

To justify one more time the framework described in Sect. 3.2, we now state the following convergence result [54,73]. Roughly speaking, it can be stated as follows : if a sequence $\mathcal{T}_k$ of triangular meshes of $\mathbb{R}^3$ tends (for a suitable topology) to a smooth surface S, then the corresponding second fundamental measures $\Phi_{\mathcal{T}_k}$, (*resp.* eigenvalues $\{\lambda_i^{\mathcal{T}_k}, (1 \leq i \leq 3)\}$), tend to Φ_S, (*resp.* $\{\lambda_i^S, (1 \leq i \leq 3)\}$). To be accurate, we will use the following terminology [54,55]:

- The *fatness* $\Theta(\mathcal{T})$ of a triangular mesh $\mathcal{T}$ is defined as follows : if t is a triangle, we begin to define the *size* $\epsilon(t)$ of t : it is the maximum of the length of its edges e. Moreover, the *fatness* of t is the real number

  $$\Theta(t) = \frac{area(t)}{\epsilon(t)^2}.$$

  Finally, the *fatness* of $\mathcal{T}$ is the minimum of the fatness of its triangles. We denote by $\mathbf{F}_\theta$ the class of triangular meshes in $\mathbb{R}^3$ with fatness greater or equal to θ.
- A triangular mesh $\mathcal{T}$ in $\mathbb{R}^3$ is *closely inscribed* in a smooth surface S if its vertices belong to S and if the orthogonal projection of $\mathcal{T}$ onto S is a bijection.

It is well known that in general, the Haussdorf convergence of a sequence of triangular mesh to a smooth surface does not imply the convergence of their geometric invariant (as shown by the classical lantern of Schwarz example [54,55]). However, adding assumptions on the fatness of the triangular meshes, one can prove the following result in [17,18,54]:

Theorem 2 *Let S be an (oriented closed) smooth surface of $\mathbb{R}^3$. Let $\mathcal{T}_k$ be a sequence of (oriented closed) triangular meshes $\mathcal{T}_k$ closely inscribed in S such that :*

1. *The limit of $\mathcal{T}_k$ is S for the Hausdorff distance,*
2. *The fatness of $\mathcal{T}_k$ is uniformly bounded by below by a positive constant : there exists $\theta > 0$ such that for all $k \in \mathbb{N}$, $\mathcal{T}_k \in \mathbf{F}_\theta$.*

Then,

1. *The sequence of second fundamental measures $\Phi_{\mathcal{T}_k}$ weakly converges to $\Phi_S = \overline{h}^S$;*
2. *The principal curvature measures $\lambda_i^{\mathcal{T}_k}$, weakly converge to the curvature measures λ_i^S, $(1 \leq i \leq 3)$.*

In particular, for any Borel subset B whose boundary is empty, and fixed X and Y, the sequence $\Phi_{\mathcal{T}_k}^{X,Y}(B)$ converges to $\Phi_S^{X,Y}(B)$, and the principal curvature measures $\lambda_i^{\mathcal{T}_k}(B)$, converge to the curvature measures $\lambda_i^S(B)$.

3.7 Principal Curvature Measures Estimated on Analytic Surfaces

In this section, some examples are introduced to show the estimation results of principal curvature measures on three analytic surfaces in triangle meshes. We first define the smooth analytic surface by its analytic formula. Then a series of points situating on the smooth surfaces are selected uniformly, and the Delaunay triangulation is performed on them to generate the triangle mesh. Three analytic surfaces are the unit sphere, the hyperbolic paraboloid and the Enneper surface presented as below and shown in Fig. 2.

Unit Sphere The smooth unit sphere is defined as

$$\begin{cases} x = r \cos\theta \sin\phi \\ y = r \sin\theta \sin\phi \\ z = r \cos\phi \end{cases} \tag{19}$$

where $r = 1$, $0 \leq \theta \leq 2\pi$ and $0 \leq \phi \leq \pi$. The corresponding meshed unit sphere contains 2,452 vertices and 4,900 triangle facets.

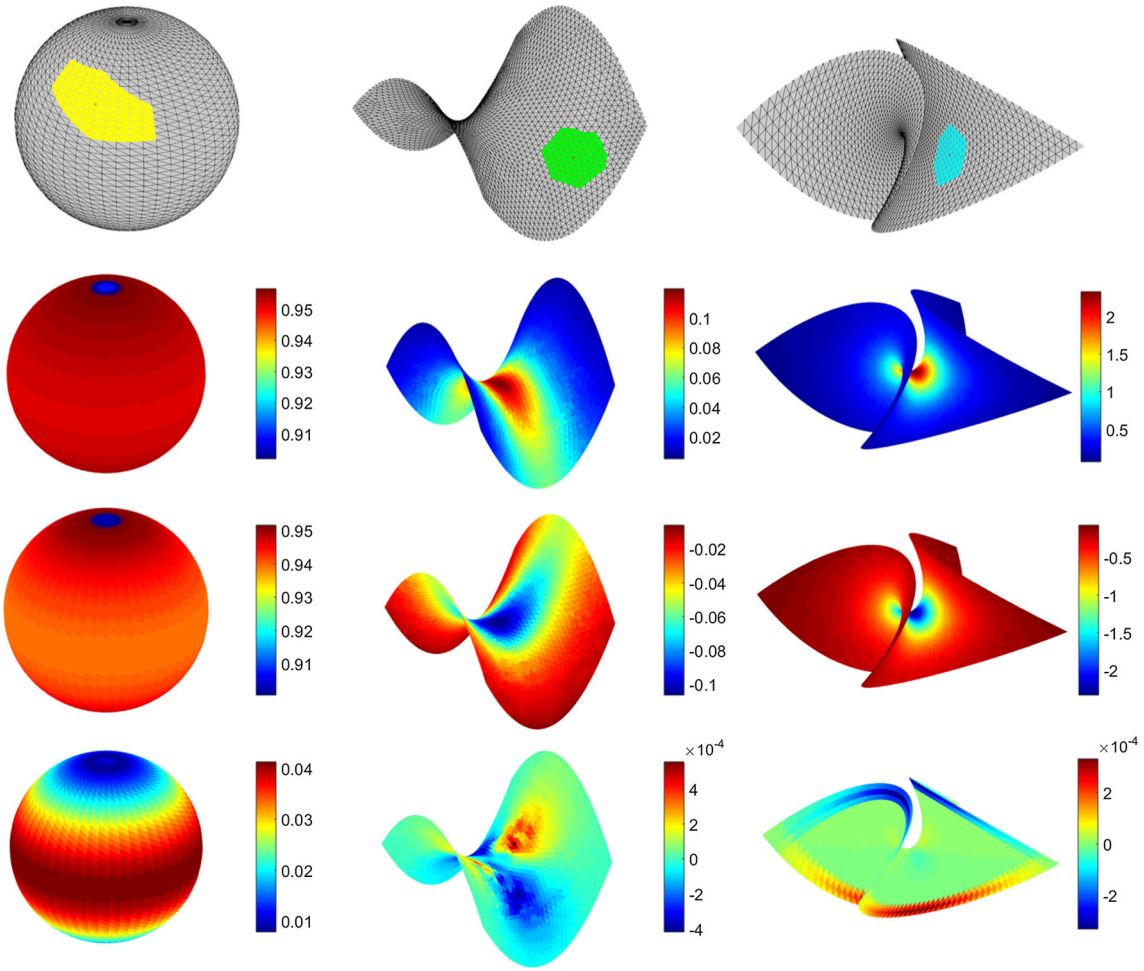

Fig. 2 Three analytic surfaces in triangle mesh (*1st row*) and three principal curvature measures estimated over the Borel subset of 5-ring (*2nd–4th rows*)

Hyperbolic Paraboloid The quadratic and doubly ruled surface given by the following Cartesian equation.

$$\begin{cases} x = u \\ y = v \\ z = \frac{u^2}{a^2} - \frac{v^2}{b^2} \end{cases} \tag{20}$$

where the parameters a is 3.71 and b is 3.89. The ranges of u and v are both $[-15, 15]$. The meshed hyperbolic paraboloid contains 2,150 vertices and 4,102 triangle facets. This model is generated by Sun in [72].

Enneper surface The parameter equation of the Enneper surface is:

$$\begin{cases} x = u - \frac{u^3}{3} + u \cdot v^2 \\ y = -(v - \frac{v^3}{3} + v \cdot u^2) \\ z = u^2 - v^2 \end{cases} \tag{21}$$

where the ranges of u and v are both $[-1.5, 1.5]$. The meshed Enneper surface contains 2,500 vertices and 4,802 triangle facets.

For estimating the principal curvature measures of each vertex, Borel subset B is chosen as a sphere-like region. The intersection region between Borel subset and triangle mesh is a k-ring neighbourhood around a vertex. Specifically, given a vertex v_i, we define the set of the k-ring neighbouring vertices around v. If the least number of edges needed to connect a vertex v_j to v_i is equal or smaller than k, v_j is in this k-ring neighbourhood. Through adjusting the value of k, we control the estimation region of principal curvature measures over the Borel subset associated to v_i. Figure 2 shows the Borel subset of 5-ring neighbourhood in three analytic surfaces.

In the lower part of Fig. 2, the estimated principal curvature measures are shown in meshed analytic surfaces. The plots from the 2nd row to the 4th row show $\lambda_1^{\mathcal{T}}(B)$, $\lambda_2^{\mathcal{T}}(B)$ and $\lambda_3^{\mathcal{T}}(B)$, respectively. From the distribution of principal curvature measures on the triangle meshes, we especially point out that the impact of topology of triangle mesh on

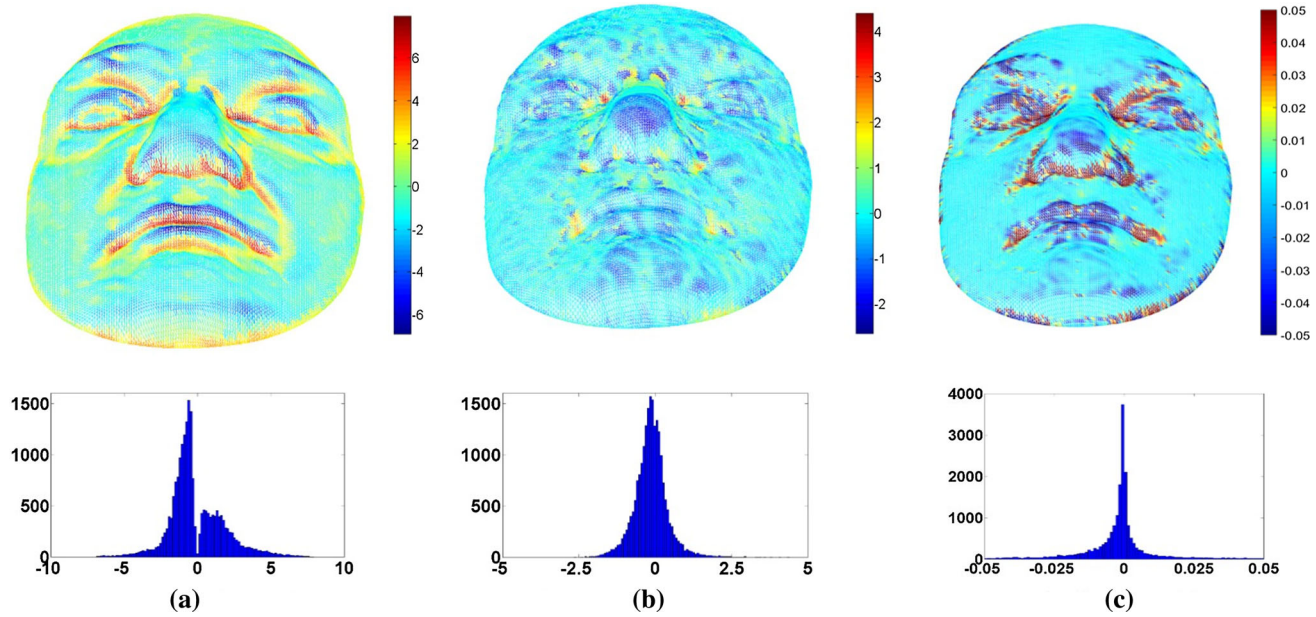

Fig. 3 Distributions of three principal curvature measures λ_{1_B}, λ_{2_B}, and λ_{3_B} calculated on a meshed 3D face scan

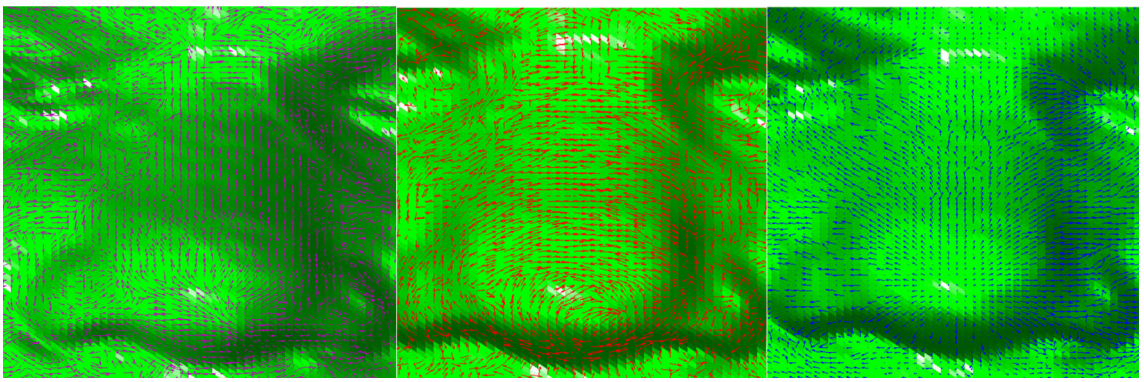

Fig. 4 Illustration of three principal curvature vectors e_{1_B}, e_{2_B}, and e_{3_B} (from *left* to *right*) calculated on a meshed 3D face scan

the estimation results. For example, principal curvatures of each point on the smooth unit sphere is homogeneous over the whole smooth surface. However, in the corresponding triangle mesh, the obvious dissimilarity exists between the principal curvature measures estimated on the vertices near the polar region and the ones estimated around the equator region. The reason is that these two regional triangle meshes have significantly different topologies, including the shape, the position, the signed angles and the distribution of the triangular facets.

3.8 Principal Curvature Measures Estimated on Meshed 3D Face Scans

Before the presentation of our designed 3D face recognition method, we show the estimation results of principal curvature measures on a 3D face scan. In our 3D face recognition approach, all the 3D face scans are typical triangle meshes. They enable us to estimate the principal curvature measures $\lambda_{1_B}^{\mathcal{T}}$, $\lambda_{2_B}^{\mathcal{T}}$, $\lambda_{3_B}^{\mathcal{T}}$ over Borel subset following the method presented in Sect. 3.5.

Figure 3 shows the principal curvature measures and their histograms on a 3D face scan in triangle mesh. We can see that the distribution of λ_{1_B} highlights the bounding of eyes and nose. The distribution of λ_{2_B} and λ_{3_B} highlight some significant feature regions (e.g. the inner and outer eye corner, the mouth corners). All three principal curvature measures are meaningful shape-based features for 3D face recognition. Figure 4 shows the principal curvature vectors of the 3D face scan.

The principal curvature measures estimated in a triangle mesh have the following threefold advantages for applying them in the shape analysis-based 3D face recognition:

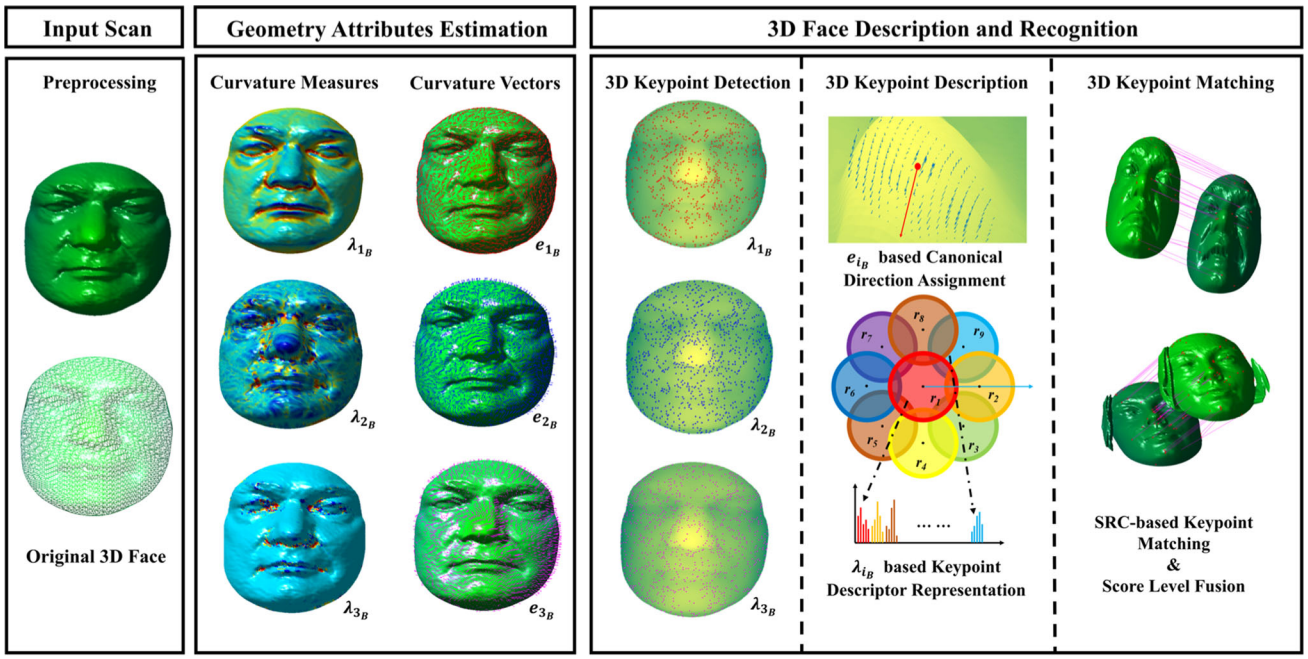

Fig. 5 Framework of principal curvature measures based 3D face description and recognition

- They can be defined and computed directly on triangle meshes. This makes the curvature-based information of a triangle mesh more reasonable and reliable. These geometric attributes represent the shape information of the original meshed 3D facial surface, rather than the manufactured surface fitting to the original meshed 3D face scan.
- In contrast to other triangle mesh-based curvature estimation methods, three principal curvature measures are achieved reasonably instead of two. Particularly, the third principle curvature measure (λ_3) enhances the description ability of facial surface. The face recognition related experimental results will show that all three principal curvature measures are useful to describe the shape of a meshed 3D face model. Furthermore, benefited by the crossing complementary shape information carried by three principal curvature measures, their combination obviously enhances the recognition performance.
- The estimation of principal curvature measures has a direct and compact association to the size of Borel subset. The adjustable Borel subset size enables these principal curvature measures to describe precisely the shape of the 3D face scans in different resolutions.

In consideration of these advantages, we will propose a 3D facial feature descriptor based on principal curvature measures and evaluate their discriminative power on comprehensive 3D face recognition experiments.

4 Principal Curvature Measures based 3D Face Description and Recognition

4.1 3D Face Description and Recognition Framework

Through studying the estimation of principal curvature measures, their significant characterization ability of discrete surfaces motivates us to apply them in practical 3D face recognition. To make full use of the rich and precise shape information represented by principal curvature measures, a promising facial feature descriptor is required. This descriptor should be effective to general 3D face recognition and robust to some uncontrollable variations. Inspired by the approaches in [29,30,40,67], we propose to create a SIFT-like feature descriptor based on principal curvature measures for 3D face recognition. As shown in Fig. 5, the description and recognition framework includes three basic modules: 3D keypoint detection, 3D keypoint description and 3D keypoint matching.

For 3D facial keypoint detection, a triangle mesh-based Gaussian scale space is firstly built to ensure the scale invariance of the keypoint description. Then, the extrema of difference of curvature (DOC), inspired from difference of Gaussian (DOG), crossing scales and one-ring neighbours are determined as qualified keypoints. Since we use three principal curvature measures, it is expected that our detection method can locate more stable and meaningful keypoints.

For 3D facial keypoint description, to comprehensively and robustly describe the local shape around a detected 3D

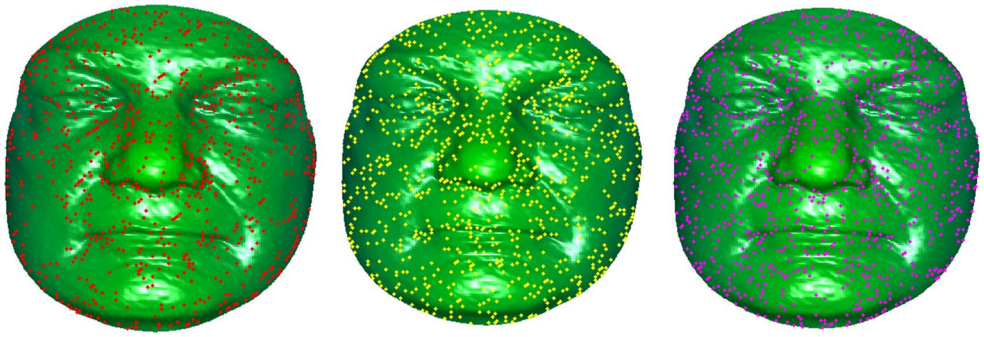

Fig. 6 Illustration of detected 3D keypoints using principal curvature measures λ_{1_B}, λ_{2_B}, and λ_{3_B} (from *left* to *right*), respectively

keypoint, we compute the histograms of all the three principal curvature measures within the neighbourhood of a detected keypoint. To make this local shape descriptor robust to head pose variations, the canonical direction is assigned for the descriptor related to the keypoint. In this approach, we propose to use the statistics of principal curvature vectors to assign the local canonical directions. This kind of 3D keypoint description is similar in spirit to the 2D SIFT [45], 2.5D SIFT [44] and meshSIFT related algorithms [48,67], but the core geometric attributes $(\lambda_{1_B}, \lambda_{2_B}, \lambda_{3_B})$ and $(e_{1_B}, e_{2_B}, e_{3_B})$ are more suitable and reasonable for the triangle mesh-based 3D facial descriptor.

For 3D facial keypoint matching, we use multi-task sparse representation [83]. This method firstly figures out the sparsest representation of each testing descriptor from the complete dictionary set built by all the descriptors in the gallery. Through solving the target sparse representation function, we obtain the corresponding sparse coefficients and the reconstruction error of the testing descriptor. Finally, the average reconstruction error of all keypoints is designed as the similarity measurement between a probe scan and a gallery scan. Thus, the identity of the testing subject is labelled as the gallery subject who has the minimum error. The details of each step are introduced in the following paragraphs.

4.2 Principal Curvature Measures for 3D Keypoint Detection

For a local feature-based descriptor, extracting descriptors only on the keypoints is the most effective method to increase the efficiency of processing. 3D keypoint detection adopted in our approach starts by performing the convolution of a given meshed 3D face scan using a series of mesh-based Gaussian convolution filters with different kernels (i.e. different scales σ_s). The original and the convolutional facial surfaces construct a Gaussian scale space to ensure the scale invariance of the facial descriptor.

Given a vertex v_i of a meshed 3D face scan $\mathcal{T}$, the Gaussian filter modifies the geometry structure of $\mathcal{T}$ over v_i's adjacent region and leads to a updated vertex $v_i^{\sigma_s}$ defined as

$$v_i^{\sigma_s} = \frac{\sum_{v_j \in N(v_i,1)} g_{\sigma_s}(v_i, v_j) \cdot v_j}{\sum_{v_j \in N(v_i,1)} g_{\sigma_s}(v_i, v_j)} \tag{22}$$

where σ_s denotes the standard deviation in scale s, $N(v_i, 1)$ denotes the set of vertices within 1-ring neighbourhood of v_i, and the Gaussian kernel g_{σ_s} is defined as

$$g_{\sigma_s}(v_i, v_j) = exp(-\left\|v_i - v_j\right\|^2 / 2\sigma_s^2) \tag{23}$$

Once the Gaussian scale space of the face scan is constructed, we estimate the principal curvature measures of Borel subset related to each vertex on the face scan in each scale. Then we compute the differences of curvature δ_i based on these principal curvature measures. The differences of curvature is defined as:

$$\delta_i(v_{\sigma_s}) = \lambda_i(B_{v_{\sigma_s}}) - \lambda_i(B_{v_{\sigma_{s-1}}}), \quad i = 1, 2, 3 \tag{24}$$

where v_{σ_s} and $v_{\sigma_{s-1}}$ denotes the updated coordinates in adjacent scales. B denotes the Borel subset of k-ring neighbourhood. 3D keypoints are determined by finding the extreme of δ_i among the surrounding vertices $v_j \in N(v_i, 1)$ in σ_s and two adjacent scales σ_{s-1} and σ_{s+1}. Once a vertex is determined as a keypoint, its detection scale is σ_s.

Figure 6 shows the detected 3D facial keypoints by using the three principal curvature measures, respectively. In each 3D face scan, the detector based on each principal curvature measure can locate around 470 keypoints numbering only 1.36% of all vertices in a whole face. It means the calculation efficiency with keypoint is 73 times theoretically faster than using all facial vertices to describe the 3D face model.

4.3 Principal Curvature Measures for 3D Keypoint Description

4.3.1 Canonical Direction Assignment

In 3D face recognition, the pose variations have intensive impact on the recognition performance of a feature descriptor by increasing significantly the intra-class distance. There are two possible solutions to handle with this problem: (1) adding a supplementary pose alignment step in the registration eliminates the interference of pose changes; (2) designing a rotation invariant local shape descriptor avoids the dissimilarity of descriptors extracted from the facial scans in different poses. In order to guarantee a higher processing efficiency, we propose to determine the canonical direction based on principal curvature vectors of each keypoint to achieve a rotation invariance descriptor remaining robust to the pose variations.

Given a meshed 3D facial surface $\mathcal{T}$, for each keypoint v_k, the vertices v_j situating in its neighbourhood are selected to become the support for assigning the canonical direction. The neighbourhood of v_k is defined as:

$$\mathcal{N}(v_k) = \{v_j \in \mathcal{T} | d_g(v_k, v_j) < R\} \tag{25}$$

where $d_g(v_k, v_j)$ denotes the geodesic distance between v_k and v_j, and R is set empirically as $9\sigma_s$ in this paper.

Then, a plane Π_{v_k} through v_k orthogonal to $e_3(B_{v_k})$ is built as a common plane for the canonical directions based on three principal curvature vectors. We choose $e_3(B)$ because its corresponding $\lambda_3(B)$ is the smallest one in three principal curvature measures, and $e_3(B)$ approximates to the normal direction, when a triangle mesh approximates to a smooth surface. Due to the principal curvature vectors of v_k are the eigenvectors of the real symmetric matrix $M_B^{\mathcal{T}}$ in (17), three principal curvature vectors are orthogonal. A local coordinate system is hence built as $(e_1(B_{v_k}), e_2(B_{v_k}), e_3(B_{v_k}))$.

All the selected v_j and their principal curvature vectors $e_i(B_{v_j})$ are transformed into this local coordinate system and further projected to Π_{v_k}, and the projections are denoted as $\tilde{v}_j$ and $\tilde{e}_i(B_{\tilde{v}_j})$, respectively. The magnitude of $\tilde{e}_i(B_{\tilde{v}_j})$, and the angle between $\tilde{e}_i(B_{\tilde{v}_j})$ and $e_1(B_{v_k})$ are defined as:

$$\begin{aligned} mag(\tilde{e}_i(B_{\tilde{v}_j})) &= \sqrt{\tilde{e}_i^x(B_{\tilde{v}_j})^2 + \tilde{e}_i^y(B_{\tilde{v}_j})^2} \\ \theta(\tilde{e}_i(B_{\tilde{v}_j})) &= arctan(\tilde{e}_i^y(B_{\tilde{v}_j}) / \tilde{e}_i^x(B_{\tilde{v}_j})), \end{aligned} \tag{26}$$

where $\tilde{e}_i^x(B_{\tilde{v}_j}) = e_1(B_{v_k}) \cdot \tilde{e}_i(B_{\tilde{v}_j})$ and $\tilde{e}_i^y(B_{\tilde{v}_j}) = e_2(B_{v_k}) \cdot \tilde{e}_i(B_{\tilde{v}_j})$.

Finally, we build a weighted histogram of $\theta(\tilde{e}_i(B_{\tilde{v}_j}))$, and divide it into 360 bins (1 bin per 1°). The weight $w(\tilde{v}_j)$ is defined as:

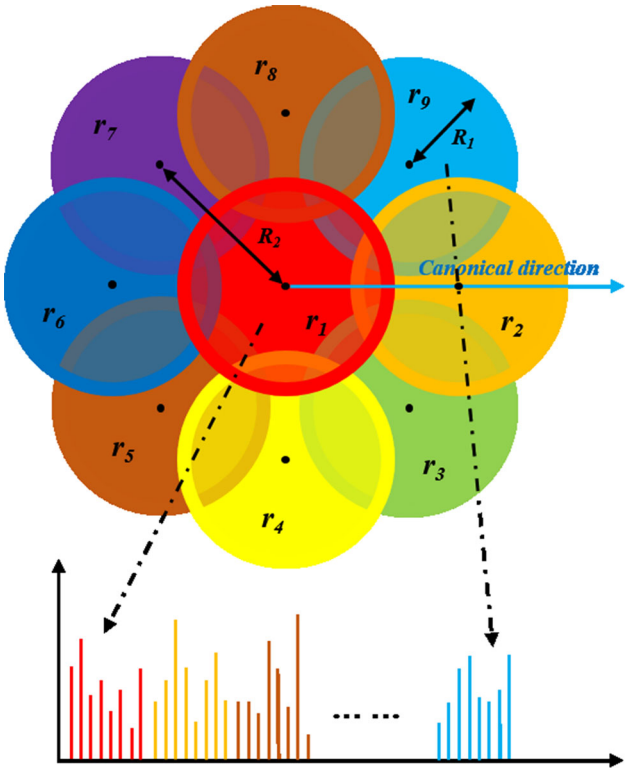

Fig. 7 3D keypoint descriptor configuration and representation

$$w(\tilde{v}_j) = mag(\tilde{e}_i(B_{\tilde{v}_j})) \cdot g(d_e(\tilde{v}_j, v_k)), \tag{27}$$

where g denotes the Gaussian kernel with the standard deviation set as half of R, and $d_e(\tilde{v}_j, v_k)$ denotes the Euclidean distance between $\tilde{v}_j$ and v_k. $e_i(B_{v_k})$ based canonical direction $\mathbf{d}_i(v_k)$ is assigned as the peak of the weighted direction histogram. Finally, for each keypoint v_k, we achieve three canonical directions $\mathbf{d}_i(v_k)$, which will be used for building the local shape descriptors based on λ_{i_B}, respectively.

In the following keypoint description step, we will extract 9 histograms in 9 neighbouring circular regions around the keypoint and generate the local descriptor by jointing them together. These 9 regions also situate in the plane Π_{v_k}. The canonical direction will be used to define the locations of these regions for guaranteeing the direction invariance of the local descriptor. It is the reason that the canonical direction assigned here lies in the projected plane Π_{v_k} rather than in $\mathbb{R}^3$.

4.3.2 3D Keypoint Descriptor Configuration

The configuration of $\lambda_i(B_{v_k})$ based descriptor is performed on the plane Π_{v_k}. Inspired by the 2D daisy descriptor [81], for each keypoint v_k, we define 9 overlapping circular regions r_1-r_9, as shown in Fig. 7, with a radius of R_1, the centre at the keypoint c_1 and its 8 neighbouring points c_2-c_9. Starting from the canonical direction $\mathbf{d}_i(v_k)$, the 8 neighbouring points are

localized around by performing a uniform sampling circle centred at v_k with a radius of R_2.

This kind of quasi-daisy radial flower pattern of overlapping circles simulates the functioning of human complex cells in the visual cortex [36]. The parameter R_1 is used to control the overlapping regions of the 9 circles for feature pooling. As shown in [81], this pattern tends to be robust to small transformations, e.g. spatial shifting or non-rigid deformations. Thus, it is better to set the parameters to satisfy $2R_1 > R_2$. Furthermore, the value of R_2 offers a trade off between descriptiveness and sensitivity to variations, e.g. facial expression. Generally, local surface descriptors with smaller size are more robust to various variations, while too small values of radii will decrease the descriptiveness of the descriptor as stated in [52]. Based on the above principals, in this paper, we set R_1 and R_2 to be $3.75\sigma_s$ and $4.5\sigma_s$. A similar parameter setting has also been adopted in [38,40,67] and proved to be powerful for 3D keypoint description.

4.3.3 3D Keypoint Descriptor Representation

In each circular region r_t, $t \in \{1, 2, \ldots, 9\}$, we construct the local weighted histograms of different principal curvature measures: λ_{1_B}, λ_{2_B}, and λ_{3_B}. The histograms of r_t are referred as $hoc_1^{r_t}$, $hoc_2^{r_t}$ and $hoc_3^{r_t}$. The values of principal curvature measures are quantized equally to 8 bins, and weighted by a Gaussian kernel $g_{\sigma_s}(d_e(\tilde{v_j}, c_t))$, where the standard deviation is set as the Euclidean distance between the current point and the centre of the circle. The final descriptors related to three principal curvature measures of a keypoint are constructed by concatenating $hoc_1^{r_t}$, $hoc_2^{r_t}$ and $hoc_3^{r_t}$ in a clockwise direction, represented as:

$$\begin{aligned} HOC_1 &= (hoc_1^{r_1}, hoc_1^{r_2}, \ldots, hoc_1^{r_9}), \\ HOC_2 &= (hoc_2^{r_1}, hoc_2^{r_2}, \ldots, hoc_2^{r_9}), \\ HOC_3 &= (hoc_3^{r_1}, hoc_3^{r_2}, \ldots, hoc_3^{r_9}). \end{aligned} \tag{28}$$

The above sub-histograms (e.g. $hoc_i^{r_t}$) and histograms (e.g. HOC_i) are all normalized to unit vectors to eliminate the influence of non-uniform mesh sampling. This generates three 3D keypoint descriptors with the same dimension of 72. We will show that these three local descriptors contain strong complementary information in descriptiveness.

4.4 Sparse Representation-based Classifier for 3D Keypoint Matching and Score-Level Fusion

Based on the sparse representation based classifier (SRC) [83], Li et al. [40] proposed the SRC-based 3D keypoint matching method, which has been successfully used for 3D face recognition. To perform the SRC-based matcher, the first step is to build a dictionary, including all the 3D keypoint descriptors of the gallery samples. Given a gallery set of N subjects, each subject has a single 3D face scan. Assume that n_i 3D keypoints are detected for *i-th* subject. Let the corresponding n_i 3D keypoint descriptors be the following sub-dictionary:

$$\mathbf{D}_i = [\mathrm{d}_{i,n_1}, \mathrm{d}_{i,n_2}, \ldots, \mathrm{d}_{i,n_i}] \in \mathbb{R}^{m \times n_i}, \tag{29}$$

where m is the descriptor dimension. Then, the dictionary for all the N subjects in the gallery can be built by simply concatenating all the sub-dictionaries as:

$$\mathbf{D} = [\mathbf{D}_1, \mathbf{D}_2, \ldots, \mathbf{D}_N] \in \mathbb{R}^{m \times K}, \tag{30}$$

where $K = n_1 + n_2 + \cdots + n_N$ represents the total number of keypoint descriptors in the gallery.

Once the gallery dictionary has been constructed, one needs to solve the following multi-task sparse representation problem:

$$\arg\min_{\mathrm{x}_i} \|\mathrm{y}_i - \mathbf{D}\mathrm{x}_i\|_2 \, s.t. \, \|\mathrm{x}_i\|_0 \leq L, \; i = 1, 2, \ldots, n, \tag{31}$$

where y_i denotes i-th 3D keypoint descriptor of a probe face scan, x_i is the sparse coefficient, $\|\cdot\|_0$ denotes the l_0 norm of a vector, defined as the number of non-zero elements of the vector, and L is the sparsity parameter controlling the sparsity of the solution.

Finally, the identity of the probe face scan can be determined by the following average accumulative sparse reconstruction error, as the similarity measurement, for all the keypoints of the given probe face scan:

$$identity(\mathbf{Y}) = \arg\min_j \frac{1}{n} \sum_{i=1}^{n} \|\mathrm{y}_i - \mathrm{D}\delta_j(\hat{\mathrm{x}}_i)\|_2^2, \tag{32}$$

where $\delta_j(\cdot)$ is a characteristic function which selects only the coefficients associated with the j-th subject.

As aforementioned, three principal curvature measures and vectors are used to form three feature descriptors. We combine their similarity measurements with the score-level fusion rules to consider all their contributions for the final decision step.

5 Experiments

To see the accuracy of estimating principal curvature measures on triangle meshes, we estimated them on three meshed analytic surfaces introduced in Sect. 3.7 and compared them to the corresponding results computed on the smooth analytic surfaces. To demonstrate the effectiveness of the proposed method for 3D face recognition, we employed three public databases for experiments, i.e. FRGC v2.0 [59], Bosphorus

Table 1 Average absolute difference and maximum absolute difference of principal curvature measures estimated on meshed and smooth analytic surfaces with different sizes of Borel subset

Borel subset size	Unit sphere			Hyperbolic paraboloid			Enneper surface		
	λ_{1_B}	λ_{2_B}	λ_{3_B}	λ_{1_B}	λ_{2_B}	λ_{3_B}	λ_{1_B}	λ_{2_B}	λ_{3_B}
Average absolute difference									
3-ring	0.05044	0.05874	0.02518	0.00543	0.00532	0.000005	0.09425	0.09425	3.4e−14
5-ring	0.03477	0.05462	0.07225	0.00424	0.00418	0.000019	0.06824	0.06824	6.5e−14
7-ring	0.03279	0.06781	0.13827	0.00448	0.00444	0.000035	0.02702	0.02702	2.1e−13
Maximum absolute difference									
3-ring	0.09808	0.09938	0.04127	0.01701	0.01782	0.00055	0.42876	0.42876	0.00032
5-ring	0.05178	0.06857	0.11605	0.01365	0.01342	0.00081	0.37721	0.37721	0.00136
7-ring	0.04662	0.09687	0.21568	0.01459	0.01491	0.00126	0.20590	0.20590	0.00366

[64], and Gavab DB [53]. The first is to evaluate performance with large number of subjects involving near-frontal face and various facial expression variations; the second is to observe its robustness to head pose variations and external facial occlusions; while the last one is to further analyse the recognition accuracy on 3D face scans with extreme expression and pose changes (left and right profiles).

5.1 Estimation of Principal Curvature Measures on Meshed Analytic Surfaces

For each meshed analytic surface $\mathcal{T}$ produced in Sect. 3.7, we compute $\lambda_i^T(B_v)$ ($i \in \{1,2,3\}$) associated to the Borel subset centering at each vertex v. k-ring neighbouring region ($\mathcal{T} \bigcap B$) of v denotes the size of Borel subset B_v. Moreover, because all vertices used to produce meshed analytic surface are selected on the corresponding smooth analytic surface S (see Sect. 3.7), one can certainly find a point $p \in S$ corresponding to $v \in \mathcal{T}$ who possess the same position. For this kind of $p \in S$, we further compute its $\lambda_i^S(B_p)$ ($i \in \{1,2,3\}$) over Borel subset associated to point p, by using the following method:

$$\lambda_i^S(B_p) = \int_{q \in B_p} \lambda_{i_q} dq, \quad i \in \{1,2,3\}, \tag{33}$$

where B_p denotes the corresponding region utilized in the triangle mesh, q is the point on the smooth analytic surface. λ_{1_q} and λ_{2_q} are the principal curvatures computed on smooth surface using traditional formula, while λ_{3_q} is 0.

To compare $\lambda_i^T(B_v)$ and $\lambda_i^S(B_p)$, we define the average absolute difference Δ^{avg} and the maximum absolute difference $\Delta^{\max}$ as

$$\begin{aligned} \Delta_i^{\text{avg}} &= \frac{1}{n}\sum_{j=1}^{n}\left|\lambda_i^T(B(v_j)) - \lambda_i^S(B(p_j))\right|, \\ \Delta_i^{\max} &= \max_{j\in\{1,2,\ldots,n\}}\left\{\left|\lambda_i^T(B(v_j)) - \lambda_i^S(B(p_j))\right|\right\}. \end{aligned} \tag{34}$$

where $i \in 1,2,3$ and n is the number of vertices on meshed surfaces and corresponding points on smooth surface.

Table 1 lists Δ^{avg} and $\Delta^{\max}$ associated to three Borel subsets, i.e. 3-ring, 5-ring, and 7-ring neighbourhood. The Δ^{avg} of unit sphere, hyperbolic paraboloid and Enneper surface are, respectively, around 0.05, 0.004 and 0.07. They demonstrate that the estimated principal curvature measures approximate to the principal curvatures calculated on each smooth analytic surface. For each analytic surface, using Borel subset of 5-ring to estimate achieves smaller Δ^{avg} and $\Delta^{\max}$. It indicates that this size of Borel subset is most suitable to estimate principal curvature measures in these meshed analytic surfaces.

5.2 Experiments on the FRGC v2.0 Database

5.2.1 Database and Protocol Description

The FRGC v2.0 database [59] is one of the most comprehensive and popular benchmark databases in the literature of 3D face recognition. It consists of 4007 meshed 3D face scans of 466 subjects with both genders, various ages, and different ethnicities. These 3D face scans, with a geometric accuracy of 0.05 mm, were captured by the Minolta Vivid 900 3D scanner. A preprocessing step proposed in [75] was used for each raw 3D face scan to remove noises, fill holes and detect nose tip.

Thanks to the pose invariance of our principle curvature measures and their corresponding local surface descriptors, we did not perform any registration on these meshed 3D face scans, in contrast to most works such as [4,70,82]. Each 3D face scan was automatically cropped by a sphere centre at the nose tip with a radius of 90 mm, resulting a triangle mesh containing about 30,000 vertexes and 40,000 facets in average. Figure 8 shows some preprocessed samples of different subjects for the following recognition work.

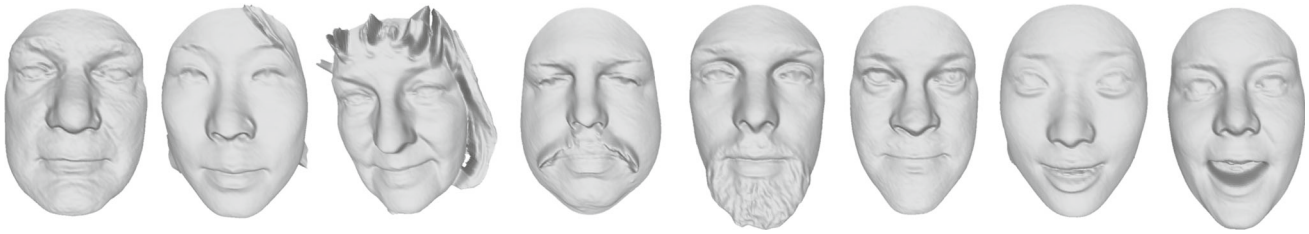

Fig. 8 Examples of the preprocessed mesh-based 3D face scans of different subjects with various facial expressions, near-frontal head poses and occlusions by hairs or beards

We evaluated the proposed method in both face identification and face verification scenarios. To make a fair comparison with the state-of-the-art methods, we adopt the same experimental protocol that the first 3D face scan from each subject groups a gallery of 466 samples and the remaining 3541 samples are labelled as probes. The probe samples were further split into two subsets according to their facial expression labels to evaluate the robustness to facial expression variations. The first subset includes all the neutral samples and the other one contains samples with non-neutral facial expressions. Thus, three experiments: *Neutral versus All*, *Neutral versus Neutral*, and *Neutral versus Non-neutral* were conducted based on the whole probe set, the neutral subset and the non-neutral subset, respectively. The verification experiment is carried on the *All versus All* scenario, which is defined over the square similarity matrix with a dimension 4007×4007.

To guarantee the robustness of principle curvature measure estimation on 3D face scans, we compared three different sizes of Borel subset, namely 3-ring, 5-ring, and 7-ring, respectively. In each case, we constructed their corresponding local shape descriptors: HOC_1, HOC_2, and HOC_3, respectively. To analyse the complementarity among these descriptors involving the same k-ring, three different score-level fusions, i.e. sum rule, production rule, and minimum rule, were tested.

In the following experiments, as well as the ones carried out the Bosphorus and Gavab databases, we empirically adopt the parameters as follows. For 3D keypoint detection, Gaussian kernel related parameter σ_s is set as 1.83, 2.58, 3.66 and 5.17 mm. The sparse parameter L is set as 3 for 3D keypoint matching.

5.2.2 Performance of Individual Curvature-Based Descriptors

The first experiment was carried on the *Neutral versus All* subset with each single descriptor. From the results listed in Table 2, it is easy to see that the size of Borel subset indeed has marginally impact on the discriminative power of individual descriptor for 3D face recognition. All the three descriptors (HOC_1, HOC_2, and HOC_3) perform best in the case of 5-ring, with gains from 0.77 to 2.80%. Based on this finding, the Borel subset size is set to be 5-ring for all the following experiments in this paper.

Table 2 Rank-one recognition rates of individual curvature-based descriptors on the whole FRGC v2.0 database

Size of Borel subset	3-ring (%)	5-ring (%)	7-ring (%)
HOC_1	91.34	**92.62**	90.07
HOC_2	83.20	**85.49**	83.71
HOC_3	84.47	**85.24**	82.44

Bold values indicate the highest or the best experimental results in the counterpart results

In the case of 5-ring, all the three descriptors can achieve interesting performance, that is, 92.62, 85.49, and 85.24% for HOC_1, HOC_2 and HOC_3, respectively. These results indicate that the proposed principle curvature measures have large potential to be efficiently used for 3D facial surface characterization and recognition. Moreover, HOC_1 performs much better (more than 7%) than HOC_2 and HOC_3, which means the first principle curvature measure (i.e. the largest eigenvalue of the second fundamental measure) is capable to encode much more shape information than the other two. Readers can also refer to Fig. 4 to see the distribution differences of the three principle curvature measures.

5.2.3 Complementarity Among Different Curvature-Based Descriptors

According to the finding that different principle curvature measure has different distribution on 3D face, we guess that different curvatures can highlight different local facial regions and their related descriptor also has some special responses to different facial shapes. In other words, the three curvature measures contain large complementary information. Thus, if we combine different curvature-based descriptors, it is expected to ameliorate the recognition performance synchronously. To verify our guess, we fused these curvature-based descriptors by three fusion rules: sum rule, product rule, and minimum rule.

In Table 3, for all three fusion rules, the rank-one recognition scores achieved by fusing any two or three curvature-

Table 3 Rank-one recognition rates of score-level fusion of curvature-based descriptors on the whole FRGC v2.0 database

Fusion rules	Sum (%)	Product (%)	Minimum (%)
$HOC_1 + HOC_2$	**95.42**	95.42	94.90
$HOC_2 + HOC_3$	**93.64**	91.35	91.09
$HOC_3 + HOC_1$	**97.20**	95.92	95.17
$HOC_1 + HOC_2 + HOC_3$	**97.96**	97.20	97.46

Bold values indicate the highest or the best experimental results in the counterpart results

Table 4 Rank-one performance comparison using the expression protocol on the FRGC v2.0 database

	Subset I (%)	Subset II (%)	Degradation (%)
Mian et al. [52]	99.0	86.7	12.3
Huang et al. [35]	99.1	92.5	6.6
Alyuz et al. [1]	98.4	**96.4**	**2.0**
Huang et al. [34]	99.2	95.1	4.1
Li et al. [40]	98.7	93.3	5.4
Our method	**99.6**	**95.7**	**3.9**

Bold values indicate the highest or the best experimental results in the counterpart results
Subset I: neutral versus neutral; Subset II: neutral versus non-neutral

base descriptors are significantly higher than the ones of each single descriptor. The fusion score of HOC_2 and HOC_3 is improved to 93.64% from 85.49 and 85.24% of HOC_2 and HOC_3, respectively. This indicates that the second and the third principle curvature measures have considerable complementarity for 3D face description. Moreover, the sum rule always performs the best for all fusion cases. This suggests us to use the sum rule for descriptor fusion in our following experiments.

5.2.4 Robustness to Facial Expression Changes

We further performed the experiments based on the expression protocol used in the other approaches, and compared the rank-one scores of our proposed method to theirs for the robustness analysis of facial expression variations (see Table 4). The results of our method are 99.6 and 95.7% for the *Neutral verse Neutral* (Subset I) and *Neutral verse Non-neutral* (Subset II) experiments, respectively. Compared with the other state-of-the-art approaches, these scores achieved the best in Subset I and rank the second in Subset II. Noting that the slight higher score achieved by [1] on Subset II depends on a region-based facial registration algorithm, while our method is totally registration free. The degradation of our method is only 3.9%, which indicates that it is robust to moderate facial expression changes.

Table 5 Performance comparison on the FRGC v2.0 database

	Data format	R1RR (%)	TAR (%)
Chang et al. [14]	Range	91.90	–
Mian et al. [51]	Range	95.73	98.31
Kakadiaris et al. [37]	Range	97.00	97.30
Wang et al. [82]	Range	**98.30**	97.97
Spreeuwers et al. [70]	Range	**99.00**	94.60
Huang et al. [33]	Range	97.20	98.40
Spreeuwers [71]	Range	**99.40**	**99.30**
Ballihi et al. [4]	Mesh	**98.02**	–
Li et al. [40]	Mesh	96.30	–
Smeets et al. [67]	Mesh	89.60	78.97
Tang et al. [78]	Mesh	93.16	93.33
Proposed method	Mesh	**97.96**	95.28

Bold values indicate the highest or the best experimental results in the counterpart results
R1RR rank-one recognition rate, TAR true accept rate is reported for FAR = 0.1%

5.2.5 Comparison with Other Approaches

To further demonstrate the effectiveness of the proposed approach, we compared it with the state-of-the-art ones in both face identification and verification scenarios on the whole FRGC v2.0 database (see Table 5).

From Table 5, we can conclude that: (1) For face identification, the rank-one recognition rate achieved by the proposed approach is comparable to the ones of the best range-based approaches (e.g. [71,82]), and ranks the second among the mesh-based approaches. However, all these methods need sophisticated and time-consuming 3D face registration step while ours skips it. Moreover, all the range-based methods, as well as the mesh-based one [4], cannot automatically deal with 3D faces with extreme pose variations (e.g. left and right profiles), which will be considered to test with our method in the following experiments on the other two databases. When focusing on the curvature-based methods in [40,67,78], our method achieves the best performance. (2) For face verification, our method also achieves the best verification rate (TAR) of 95.28% with FAR=0.1% among all the mesh-based methods. In Fig. 9, we also show that the fusions of different curvature-based descriptors can also largely improve the face verification rates.

5.3 Experiments on the Bosphorus Database

5.3.1 Database and Protocol Description

Bosphorus database [64] is quite unique for its broad set of expression types, systematic variation of poses and different types of external occlusions, which may typically occur in the

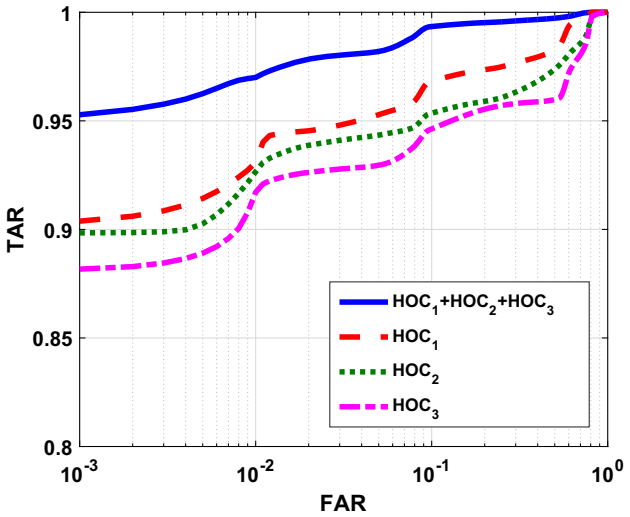

Fig. 9 ROC curves display the effectiveness of the fusion of different curvature-based descriptors in the verification scenarios

Table 6 Rank-one recognition rate with pose and occlusion variations on the Bosphorus database

	HOC_1 (%)	HOC_2 (%)	HOC_3 (%)	Fusion (%)
YR 10° (105)	100	100	100	**100**
YR 20° (105)	99.05	98.10	97.14	**99.05**
YR 30° (105)	97.14	98.10	94.29	**99.05**
YR 45° (210)	96.19	94.29	92.86	**98.57**
YR 90° (210)	49.67	36.19	20.00	**57.14**
PR (419)	98.33	97.61	95.94	**99.52**
CR (211)	97.16	95.73	92.89	**99.05**
Overall	89.96	87.62	83.59	**92.75**
HandE (105)	98.10	97.14	94.29	**100**
HandM (105)	100	99.05	97.14	**100**
Glasses (104)	96.15	94.23	88.46	**97.12**
Hair (67)	92.54	86.57	76.12	**95.52**
Overall	97.11	95.01	90.29	**98.43**

Bold values indicate the highest or the best experimental results in the counterpart results

real-life application under uncontrolled environment. Specifically, it contains 4666 face scans of 105 subjects, involving 44 women and 61 men. For each subject, there are around 34 expressions, 7 poses and 4 occlusions. All 3D face scans were captured by Inspeck Mega Capturor II 3D digitizer device, which has about 0.3 mm sensor resolution in all x, y and z dimensions. After the preprocessing steps of manually facial region segmentation, noise removing, and down-sampling, each mesh-based 3D face scan contains approximately 35K vertices. Figure 10 displays some samples with different head pose variations and external occlusions.

On this database, we only conduct the face identification experiment. In particular, we take 105 neutral samples in frontal view from each subject to construct the gallery set. To demonstrate the robustness of the proposed method for pose and occlusion variations, two subsets, namely *pose subset* and *occlusion subset* were used as the probe sets, respectively. The *pose subset* contains 1365 face samples of 105 subjects with 7 types of Yaw Rotations (YR) from 10 degree to 90 degree, 4 types of Pitch Rotations (PR), and 2 kinds of Cross Rotations (CR). The *occlusion subset* includes 381 3D face scans with 2 types of external occlusions by glasses (Glasses) and hair (Hair), and 2 types of occlusions on eye and mouth by hand (HandE and HandM).

5.3.2 Robustness to Pose and Occlusion Variations

Table 6 lists the rank-one recognition rates of the proposed method on the Bosphorus database. On the performance of each single curvature-based descriptor and their score-level fusion, we can get similar conclusions, that is, HOC_1 performs better than HOC_2 and HOC_3 in almost all subsets, and the score-level fusion of all three descriptors can significantly improve the recognition rates.

Robustness to pose changes As shown in the upper part of Table 6, in the cases of the Yaw rotations no more than 30°, as well as all the Pitch rotations and the Cross rotations, our proposed method achieves the recognition rates more than 99%, illustrating its effectiveness to recognize the faces under moderate pose changes. Faces rotate around 45°, the proposed method can also recognize correctly 98.57% of samples. Even in the extreme large rotation case (YR 90°), the rate remains still more than 50%. These results illustrate that

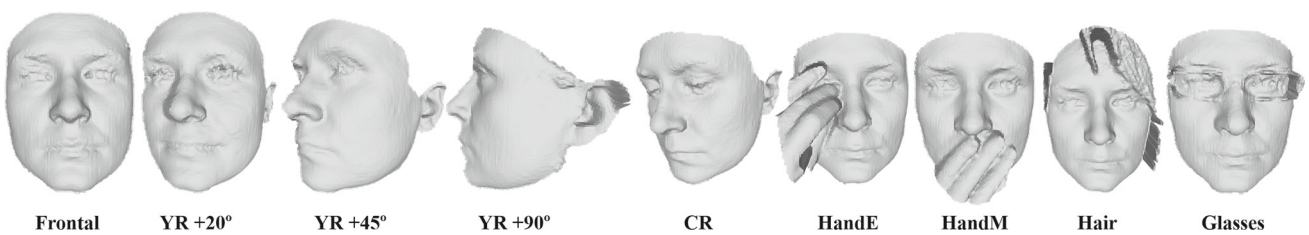

Fig. 10 Examples of the mesh-based 3D face scans in the Bosphorus database: the faces of the same subject with various changes of head poses and occlusions are illustrated

Table 7 Performance comparison on the pose subset of the Bosphorus database

	YR 10° (%)	YR 20° (%)	YR 30° (%)	YR 45° (%)	YR 90° (%)	PR (%)	CR (%)	Overall (%)
Dibeklioglu et al. [21]	–	–	–	–	–	–	–	79.41
Maes et al. [48]	–	–	–	85.6	24.3	–	–	84.2
Hajati et al. [31]	92.3	88.6	80.0	38.6	–	–	–	69.1
Berretti et al. [6]	–	–	–	–	45.7	98.3	93.2	88.55
Li et al. [40]	100	**100**	99.1	97.6	47.1	99.5	99.1	91.1
Our method	**100**	99.1	**99.1**	**98.6**	**57.1**	**99.5**	**99.1**	**92.8**

Bold values indicate the highest or the best experimental results in the counterpart results

Table 8 Performance comparison on the occlusion subset of the Bosphorus database

	(a) %	(b) %	(c) %	(d) %	(e) %
Alyuz et al. [2]	93.6	93.6	97.8	89.6	93.6
Colobo et al. [19]	91.1	74.7	94.2	90.4	87.6
Drira et al. [24]	97.1	78.0	94.2	81.0	87.0
Li et al. [40]	100	**100**	100	95.5	**99.2**
Our method	**100**	**100**	97.12	**95.5**	98.4

Bold values indicate the highest or the best experimental results in the counterpart results
(a) HandE, (b) HandM, (c) Glasses, (d) Hair, (e) Overall

our proposed descriptor is robust to various pose changes, especially to the cases that the single or complex rotations are no more than 45°.

Robustness to occlusions As shown in the lower part of Table 6, the proposed method is also very robust to the variations of external occlusions. When the occlusion is caused by hand, the recognition rates are around 97% even using a single descriptor, and raised to 100% when fusing three descriptors. It indicates that if the occlusion is not caused by excessive pose changes, our method can remain a high performance even a part of face is missing. Another interesting finding is that, if the mouth is hidden (HandM), the recognition rate is higher than the one when the eye is hidden (HandE). We surmise that the eye surrounding area can provide richer shape information than the lower part of the face for 3D face recognition. For the cases of glasses and hair occlusions, the recognition rates degrade a bit to 97.12% and 95.52%. The long hair of female covering the major part of face increases obviously the recognition complication.

5.3.3 Comparison with Other Approaches

Table 7 compares the proposed method with the state-of-the-art ones on the pose subset. Hajati et al. [31] reported an approach using patch geodesic moments which are extracted from the texture image controlled by the corresponding range image. However, the cropping, pose correction and alignment in their method were performed manually. Li et al. [40] proposed the multi-order surface differential quantities based method, which is robust to expression, pose and occlusion variations. Comparatively, our proposed method achieves equal or better results in almost all parts of this subset, except the case of YR 20°. It further shows the robustness of our method to diverse pose changes.

Table 8 compares our method with the state-of-the-art approaches on the occlusion subset. In [19] and [24], the learning-based methods (e.g. face subspace related method) were adopted for occlusion detection and missing face restoration. However, the training samples used to build the face subspace need to be correctly and carefully normalized. Our proposed method, without any prior training and alignment, outperforms these methods. It also achieves the same rank-one scores as [40] in the cases of occlusions caused by hand and hair. That is, 100%, 100%, and 95.5% on the subsets of HandE, HandM and Hair, respectively. In the case of glass occlusion, there are only three samples which are not correctly recognized by our method.

5.4 Experiments on the Gavab Database

5.4.1 Database and Protocol Description

The Gavab database [53] comprises many noisy 3D face scans with large pose and expression variations captured by Minolta Vi-700. This database consists of 61 adult Caucasian individuals (45 males and 16 females). For each individual, nine scans are taken in different acquisition viewpoints and facial expressions, resulting in 549 facial scans. In particular, there are two frontal face scans with neutral expression, two face scans captured while the subject is looking up or looking down (around 35°) with neutral expression, three frontal scans in which the subject smiles, laughs, or shows a random expression, and two profile scans with a rotation of 90° left and right. Figure 11 shows some samples of the same subjects with various variations of facial expressions and head poses. We conduct face identification task on the whole Gavab database. A similar preprocessing step was utilized as in the FRGC v2.0 database to remove spikes and

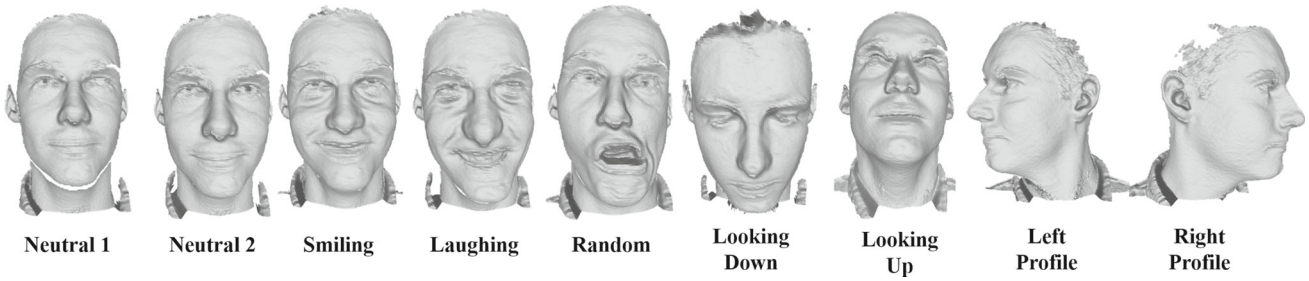

Fig. 11 Examples in the Gavab database: the mesh-based 3D face scans of the same subjects with various variations of facial expressions and head poses are illustrated

Table 9 Comparison of rank-one recognition rates on the Gavab database

	A (%)	B (%)	C (%)	D (%)	E (%)
Amberg et al. [3]	98.1	**99.7**	–	–	–
Li et al. [42]	96.7	93.3	–	–	–
Mahoor et al. [49]	95.0	–	88.6	85.3	–
Drira et al. [24]	100	94.5	100	98.4	78.7
Berretti et al. [6]	100	94.0	96.7	95.1	**88.5**
Our method	**100**	79.2	**100**	**98.4**	86.9

Bold values indicate the highest or the best experimental results in the counterpart results
A: Neutral (61), B: Expressive (183), C: Looking up (61), D: Looking down (61), E: Profile (122)

fill holes. For each subject, we randomly choose one of the neutral face scan in frontal view to group the gallery, and all the remaining face scans are used as probes.

5.4.2 Experimental Results

Table 9 reports the rank-one recognition rates of the proposed method and the other state-of-the-art ones achieved on different subsets of the Gavab database. Our method achieves 100% recognition rate identifying frontal and looking up faces in neutral expression. When faces are under intensive expressions (random sample shown in Fig. 11), the topology of the local triangle mesh in non-rigid facial regions (cheeks and mouth) change extremely. It leads to different calculation results of principal curvature measures and related descriptors, and further decreases the accuracy. However, due to the rotation invariance of the proposed descriptor, our proposed method achieves competitive results of 100, 98.36 and 86.88% in the cases of Looking up, Looking down and Profile, respectively. In the case of extreme pose variations (Profile), our method achieves better result than [24], and slightly lower performance (two more samples are wrongly recognized by our method) than [6]. It is worth noting that our method achieves 11.4% higher rank-one recognition rate than [6] in the case of YR 90° for 210 samples on the Bosphorus database (see Table 7).

5.5 Experiment Summary

In the Sects. 5.1, 5.2, 5.3, and 5.4, nine experiments (Tables 1, 2, 3, 4, 5, 6, 7, 8, 9) are carried out on three meshed analytic surfaces (unit sphere, hyperbolic paraboloid, and Enneper surface) and three public databases, i.e. FRGC v2.0, Bosphorus and Gavab. The experimental results in Tables 1, 2, 3 show that principle curvature measures can be well estimated on both meshed analytic surfaces and real 3D face scans with Borel subset of 5-ring. Moreover, these curvature-based descriptors contain considerable complementary informations for 3D face description and recognition. The experimental results on the FRGC v2.0 database shown in Tables 4 and 5 demonstrate that our method is robust to moderate facial expression variations. Further experimental results on the Bosphorus and Gavab databases reported in Tables 6, 7, 8, and 9 indicate that the proposed curvature-based descriptors are also effective and robust to varies head pose variations (even in the cases of profiles) and external occlusions.

At the same time, we also tested the time cost of the proposed method according to the experiments conducted on the FRGC v2.0 database, where each 3D face scan contains 30 K vertices and 470 3D facial keypoints in average. Performed on a PC with Intel Core i7-3770 CPU (8 cores, 3.40 GHz) and 16 GB RAM, our unoptimized MATLAB code takes about 52.2 s (6.6, 43 and 2.6 s for keypoint detection, description and matching, respectively) to complete the whole recognition framework of a probe 3D face scan against all the 466 scans in the gallery. The main cost for the keypoint description is the computation of the geodesic neighbourhood, which can be reduced to 5.3 s with parallel computation because the processing of keypoints are independent.

6 Conclusion

We have presented an effective approach for 3D face recognition based on a novel principle curvature measure-based framework consisting of keypoint detection, description and

matching. The principle curvature measures are generalized principle curvatures defined on Borel subset of both smooth and discrete surfaces (meshed 3D face scans). The strong complementarity among different principle curvature measures provides us discriminative and complete facial shape representations. The pose invariance of the feature description based on principal curvature measures and the local feature matching make our method totally registration free in contrast to most existing 3D face recognition approaches. The proposed method achieved recognition rates of 97.96% on the whole FRGC v2.0 database, and a degradation of 3.9% between the neutral and the non-neutral expression subsets. These results demonstrate that the proposed method is robust to moderate facial expression variations. Additional experiments on the Bosphorus and Gavab databases further show that the proposed method is also robust to varies head pose variations and external occlusions, especially for extreme poses, e.g. left or right profiles.

In the future, we plan to introduce this principal curvature measure-based descriptors into more 3D face recognition challenges, e.g. 3D anti-spoofing face recognition and 3D face recognition with resolution changes.

Acknowledgements This work was supported in part by the French research agency, l'Agence Nationale de Recherche (ANR), through the Biofence project under the Grant ANR-13-INSE-0004-02. Huibin Li was supported in part by the National Natural Science Foundation of China (NSFC) under Grant No. 11401464, the China Postdoctoral Science Foundation (No. 2014M560785), and the International Exchange Funds for the Central Universities No. 2014gjhz07.

References

1. Alyuz, N., Gokberk, B., Akarun, L.: Regional registration for expression resistant 3-d face recognition. IEEE Trans. Inf. Forensics Secur. **5**(3), 425–440 (2010)
2. Alyüz, N., Gökberk, B., Dibeklioğlu, H., Savran, A., Salah, A.A., Akarun, L., Sankur, B.: 3D face recognition benchmarks on the bosphorus database with focus on facial expressions. In: European Workshop on Biometrics and Identity Management, pp. 57–66. Springer (2008)
3. Amberg, B., Knothe, R., Vetter, T.: Expression invariant 3d face recognition with a morphable model. In: IEEE International Conference on Automatic Face and Gesture Recognition, pp. 1–6. IEEE (2008)
4. Ballihi, L., Ben Amor, B., Daoudi, M., Srivastava, A., Aboutajdine, D.: Boosting 3-d-geometric features for efficient face recognition and gender classification. IEEE Trans. Inf. Forensics Secur. **7**(6), 1766–1779 (2012)
5. Berretti, S., Del Bimbo, A., Pala, P.: 3D face recognition using isogeodesic stripes. IEEE Trans. Pattern Anal. Mach. Intell. **32**(12), 2162–2177 (2010)
6. Berretti, S., Werghi, N., Del Bimbo, A., Pala, P.: Matching 3d face scans using interest points and local histogram descriptors. Comput. Graph. **37**(5), 509–525 (2013)
7. Borrelli, V., Cazals, F., Morvan, J.M.: On the angular defect of triangulations and the pointwise approximation of curvatures. Comput. Aided Geom. Des. **20**(6), 319–341 (2003)
8. Bowyer, K.W., Chang, K., Flynn, P.: A survey of approaches and challenges in 3d and multi-modal 3d+ 2d face recognition. Comput. Vis. Image Underst. **101**(1), 1–15 (2006)
9. Bronstein, A.M., Bronstein, M.M., Guibas, L.J., Ovsjanikov, M.: Shape google: geometric words and expressions for invariant shape retrieval. ACM Trans. Graph. (TOG) **30**(1), 1 (2011)
10. Bronstein, A.M., Bronstein, M.M., Kimmel, R.: Expression-invariant 3d face recognition. In: International Conference on Audio-and Video-Based Biometric Person Authentication, pp. 62–70. Springer (2003)
11. Bronstein, A.M., Bronstein, M.M., Spira, A., Kimmel, R.: Face recognition from facial surface metric. In: European Conference on Computer Vision, pp. 225–237. Springer (2004)
12. Bronstein, M.M., Kokkinos, I.: Scale-invariant heat kernel signatures for non-rigid shape recognition. In: 2010 IEEE Conference on Computer Vision and Pattern Recognition (CVPR), pp. 1704–1711. IEEE (2010)
13. Chang, K.I., Bowyer, K.W., Flynn, P.J.: Adaptive rigid multi-region selection for handling expression variation in 3d face recognition. In: IEEE Computer Society Conference on Computer Vision and Pattern Recognition Workshops, pp. 157–157 (2005)
14. Chang, K.I., Bowyer, K.W., Flynn, P.J.: Multiple nose region matching for 3d face recognition under varying facial expression. IEEE Trans. Pattern Anal. Mach. Intell. **28**(10), 1695–1700 (2006)
15. Chen, B.: Geometry of Submanifolds, vol. 22. M. Dekker (1973)
16. Chua, C.S., Jarvis, R.: Point signatures: a new representation for 3d object recognition. Int. J. Comput. Vis. **25**(1), 63–85 (1997)
17. Cohen-Steiner, D., Morvan, J.M.: Restricted delaunay triangulations and normal cycle. In: 9th Annual Symposium on Computational Geometry, pp. 312–321. ACM (2003)
18. Cohen-Steiner, D., Morvan, J.M., et al.: Second fundamental measure of geometric sets and local approximation of curvatures. J. Differ. Geom. **74**(3), 363–394 (2006)
19. Colombo, A., Cusano, C., Schettini, R.: Three-dimensional occlusion detection and restoration of partially occluded faces. J. Math. Imaging Vis. **40**(1), 105–119 (2011)
20. Conde, C., Rodríguez-Aragón, L.J., Cabello, E.: Automatic 3d face feature points extraction with spin images. In: International Conference Image Analysis and Recognition, pp. 317–328. Springer (2006)
21. Dibeklioğlu, H., Gökberk, B., Akarun, L.: Nasal region-based 3d face recognition under pose and expression variations. In: International Conference on Biometrics, pp. 309–318. Springer (2009)
22. do Carmo, M.P.: Riemannian Geometry. Birkhauser, Boston (1992)
23. Drira, H., Amor, B.B., Daoudi, M., Srivastava, A.: Pose and expression-invariant 3d face recognition using elastic radial curves. In: British Machine Vision Conference, pp. 1–11 (2010)
24. Drira, H., Amor, B.B., Srivastava, A., Daoudi, M., Slama, R.: 3D face recognition under expressions, occlusions, and pose variations. IEEE Trans. Pattern Anal. Mach. Intell. **35**(9), 2270–2283 (2013)
25. Faltemier, T.C., Bowyer, K.W., Flynn, P.J.: A region ensemble for 3-d face recognition. IEEE Trans. Inf. Forensics Secur. **3**(1), 62–73 (2008)
26. Fu, J.H.: Monge-ampere functions. Research rep./Centre for math. analysis; CMA-R16-88 (1988)
27. Goldfeather, J., Interrante, V.: A novel cubic-order algorithm for approximating principal direction vectors. ACM Trans. Graph. **23**(1), 45–63 (2004)
28. Gordon, G.G.: Face recognition based on depth and curvature features. In: IEEE Computer Society Conference on Computer Vision and Pattern Recognition., pp. 808–810 (1992)
29. Guo, Y., Bennamoun, M., Sohel, F., Lu, M., Wan, J.: 3D object recognition in cluttered scenes with local surface features: a survey. IEEE Trans. Pattern Anal. Mach. Intell. **36**(11), 2270–2287 (2014)

30. Guo, Y., Bennamoun, M., Sohel, F., Lu, M., Wan, J., Kwok, N.M.: A comprehensive performance evaluation of 3d local feature descriptors. Int. J. Comput. Vis. **116**(1), 66–89 (2016)
31. Hajati, F., Raie, A.A., Gao, Y.: 2.5D face recognition using patch geodesic moments. Pattern Recogn. **45**(3), 969–982 (2012)
32. Hamann, B.: Curvature approximation for triangulated surfaces. In: Geometric Modelling, pp. 139–153. Springer (1993)
33. Huang, D., Ardabilian, M., Wang, Y., Chen, L.: A novel geometric facial representation based on multi-scale extended local binary patterns. In: IEEE International Conference on Automatic Face and Gesture Recognition and Workshops, pp. 1–7 (2011)
34. Huang, D., Ardabilian, M., Wang, Y., Chen, L.: 3-D face recognition using eLBP-based facial description and local feature hybrid matching. IEEE Trans. Inf. Forensics Secur. **7**(5), 1551–1565 (2012)
35. Huang, D., Zhang, G., Ardabilian, M., Wang, Y., Chen, L.: 3D face recognition using distinctiveness enhanced facial representations and local feature hybrid matching. In: 2010 Fourth IEEE International Conference on Biometrics: Theory Applications and Systems (BTAS), pp. 1–7. IEEE (2010)
36. Hubel, D.H., Wiesel, T.N.: Receptive fields, binocular interaction and functional architecture in the cat's visual cortex. J. Physiol. **160**(1), 106–154 (1962)
37. Kakadiaris, I.A., Passalis, G., Toderici, G., Murtuza, M.N., Lu, Y., Karampatziakis, N., Theoharis, T.: Three-dimensional face recognition in the presence of facial expressions: an annotated deformable model approach. IEEE Trans. Pattern Anal. Mach. Intell. **29**(4), 640–649 (2007)
38. Li, H.: Towards three-dimensional face recognition in the real. Ph.D. thesis, Citeseer (2014)
39. Li, H., Huang, D., Morvan, J.M., Chen, L., Wang, Y.: Expression-robust 3d face recognition via weighted sparse representation of multi-scale and multi-component local normal patterns. Neurocomputing **133**, 179–193 (2014)
40. Li, H., Huang, D., Morvan, J.M., Wang, Y., Chen, L.: Towards 3d face recognition in the real: a registration-free approach using fine-grained matching of 3d keypoint descriptors. Int. J. Comput. Vis. **113**(2), 128–142 (2015)
41. Li, H., Zeng, W., Morvan, J.M., Chen, L., Gu, X.D.: Surface meshing with curvature convergence. IEEE Trans. Vis. Comput. Graph. **20**(6), 919–934 (2014)
42. Li, X., Jia, T., Zhang, H.: Expression-insensitive 3d face recognition using sparse representation. In: IEEE Conference on Computer Vision and Pattern Recognition, pp. 2575–2582 (2009)
43. Li, X., Zhang, H.: Adapting geometric attributes for expression-invariant 3d face recognition. In: IEEE International Conference on Shape Modeling and Applications, pp. 21–32 (2007)
44. Lo, T.W.R., Siebert, J.P.: Local feature extraction and matching on range images: 2.5D sift. Comput. Vis. Image Underst. **113**(12), 1235–1250 (2009)
45. Lowe, D.G.: Distinctive image features from scale-invariant keypoints. Int. J. Comput. Vis. **60**(2), 91–110 (2004)
46. Lu, X., Jain, A.: Deformation modeling for robust 3d face matching. IEEE Trans. Pattern Anal. Mach. Intell. **30**(8), 1346–1357 (2008)
47. Lu, X., Jain, A.K., Colbry, D.: Matching 2.5d face scans to 3d models. IEEE Trans. Pattern Anal. Mach. Intell. **28**(1), 31–43 (2006)
48. Maes, C., Fabry, T., Keustermans, J., Smeets, D., Suetens, P., Vandermeulen, D.: Feature detection on 3d face surfaces for pose normalisation and recognition. In: Fourth IEEE International Conference on Biometrics: Theory Applications and Systems, pp. 1–6 (2010)
49. Mahoor, M.H., Abdel-Mottaleb, M.: Face recognition based on 3d ridge images obtained from range data. Pattern Recogn. **42**(3), 445–451 (2009)
50. Meyer, M., Desbrun, M., Schröder, P., Barr, A.H.: Discrete differential-geometry operators for triangulated 2-manifolds. In: Visualization and Mathematics III, pp. 35–57. Springer (2003)
51. Mian, A., Bennamoun, M., Owens, R.: An efficient multimodal 2d–3d hybrid approach to automatic face recognition. IEEE Trans. Pattern Anal. Mach. Intell. **29**(11), 1927–1943 (2007)
52. Mian, A.S., Bennamoun, M., Owens, R.: Keypoint detection and local feature matching for textured 3d face recognition. Int. J. Comput. Vis. **79**(1), 1–12 (2008)
53. Moreno, A.B., Sánchez, A.: Gavabdb: a 3d face database. In: Workshop on Biometrics on the Internet, pp. 75–80 (2004)
54. Morvan, J.M.: Generalized Curvatures. Springer, Berlin (2008)
55. Morvan, J.M., Thibert, B.: Approximation of the normal vector field and the area of a smooth surface. Discret. Comput. Geom. **32**(3), 383–400 (2004)
56. Mpiperis, I., Malassiotis, S., Strintzis, M.G.: Bilinear models for 3-d face and facial expression recognition. IEEE Trans. Inf. Forensics Secur. **3**(3), 498–511 (2008)
57. Pears, N., Liu, Y., Bunting, P.: 3D imaging, analysis and applications, vol. 3. Springer, Berlin (2012)
58. Peter, W.: Normal cycle and integral curvature for polyhedra in riemannian manifolds. Differential Geometry, Colloq. Math. Soc. Janos Bolyai (1982)
59. Phillips, P.J., Flynn, P.J., Scruggs, T., Bowyer, K.W., Chang, J., Hoffman, K., Marques, J., Min, J., Worek, W.: Overview of the face recognition grand challenge. IEEE Comput. Soc. Conf. Comput. Vis. Pattern Recog. **1**, 947–954 (2005)
60. Raviv, D., Bronstein, A.M., Bronstein, M.M., Waisman, D., Sochen, N., Kimmel, R.: Equi-affine invariant geometry for shape analysis. J. Math. Imaging Vis. **50**(1–2), 144–163 (2014)
61. Razdan, A., Bae, M.: Curvature estimation scheme for triangle meshes using biquadratic bézier patches. Comput. Aided Des. **37**(14), 1481–1491 (2005)
62. Rusinkiewicz, S.: Estimating curvatures and their derivatives on triangle meshes. In: 2nd IEEE International Symposium on 3D Data Processing, Visualization and Transmission, pp. 486–493 (2004)
63. Samir, C., Srivastava, A., Daoudi, M.: Three-dimensional face recognition using shapes of facial curves. IEEE Trans. Pattern Anal. Mach. Intell. **28**(11), 1858–1863 (2006)
64. Savran, A., Alyüz, N., Dibeklioglu, H., Çeliktutan, O., Gökberk, B., Sankur, B., Akarun, L.: 3D face recognition benchmarks on the bosphorus database with focus on facial expressions. In: Workshop on Biometrics and Identity Management (2008)
65. Sharma, A., Horaud, R., Cech, J., Boyer, E.: Topologically-robust 3d shape matching based on diffusion geometry and seed growing. In: 2011 IEEE Conference on Computer Vision and Pattern Recognition (CVPR), pp. 2481–2488. IEEE (2011)
66. Smeets, D., Claes, P., Hermans, J., Vandermeulen, D., Suetens, P.: A comparative study of 3-d face recognition under expression variations. IEEE Trans. Syst. Man Cybern. C Appl. Rev. **42**(5), 710–727 (2012)
67. Smeets, D., Keustermans, J., Vandermeulen, D., Suetens, P.: Meshsift: local surface features for 3d face recognition under expression variations and partial data. Comput. Vis. Image Underst. **117**(2), 158–169 (2013)
68. Spivak, M.: Calculus on Manifolds, vol. 1. WA Benjamin, New York (1965)
69. Spivak, M.: Comprehensive Introduction to Differential Geometry, vol. 4. University of Tokyo Press, Tokyo (1981)
70. Spreeuwers, L.: Fast and accurate 3d face recognition. Int. J. Comput. Vis. **93**(3), 389–414 (2011)
71. Spreeuwers, L.: Breaking the 99% barrier: optimisation of three-dimensional face recognition. IET Biom. **4**(3), 169–178 (2015)
72. Sun, X., Morvan, J.M.: Curvature measures, normal cycles and asymptotic cones. Actes des rencontres du C.I.R.M. **3**(1), 3–10 (2013)

73. Sun, X., Morvan, J.M.: Asymptotic cones of embedded singular spaces. arXiv preprint arXiv:1501.02639 (2015)
74. Surazhsky, T., Magid, E., Soldea, O., Elber, G., Rivlin, E.: A comparison of gaussian and mean curvatures estimation methods on triangular meshes. IEEE Int. Conf. Robot. Autom. **1**, 1021–1026 (2003)
75. Szeptycki, P., Ardabilian, M., Chen, L.: A coarse-to-fine curvature analysis-based rotation invariant 3d face landmarking. In: 3rd IEEE International Conference on Biometrics: Theory, Applications, and Systems, pp. 1–6 (2009)
76. Tanaka, H.T., Ikeda, M., Chiaki, H.: Curvature-based face surface recognition using spherical correlation. principal directions for curved object recognition. In: Third IEEE International Conference on Automatic Face and Gesture Recognition, pp. 372–377 (1998)
77. Tang, H., Yin, B., Sun, Y., Hu, Y.: 3D face recognition using local binary patterns. Sig. Process. **93**(8), 2190–2198 (2013)
78. Tang, Y., Sun, X., Huang, D., Morvan, J.M., Wang, Y., Chen, L.: 3D face recognition with asymptotic cones based principal curvatures. In: IEEE International Conference on Biometrics (ICB), pp. 466–472 (2015)
79. Taubin, G.: Estimating the tensor of curvature of a surface from a polyhedral approximation. In: Fifth IEEE International Conference on Computer Vision, pp. 902–907 (1995)
80. Theisel, H., Rossi, C., Zayer, R., Seidel, H.P.: Normal based estimation of the curvature tensor for triangular meshes. In: 12th IEEE Pacific Conference on Computer Graphics and Applications, pp. 288–297 (2004)
81. Tola, E., Lepetit, V., Fua, P.: Daisy: an efficient dense descriptor applied to wide-baseline stereo. IEEE Trans. Pattern Anal. Mach. Intell. **32**(5), 815–830 (2010)
82. Wang, Y., Liu, J., Tang, X.: Robust 3d face recognition by local shape difference boosting. IEEE Trans. Pattern Anal. Mach. Intell. **32**(10), 1858–1870 (2010)
83. Wright, J., Yang, A.Y., Ganesh, A., Sastry, S.S., Ma, Y.: Robust face recognition via sparse representation. IEEE Trans. Pattern Anal. Mach. Intell. **31**(2), 210–227 (2009)
84. Wu, Z., Wang, Y., Pan, G.: 3D face recognition using local shape map. IEEE Int. Conf. Image Process. **3**, 2003–2006 (2004)
85. Xu, G., Bajaj, C.L.: Curvature computation of 2-manifolds in R k. J. Comput. Math. 681–688 (2003)
86. Xu, Z., Xu, G.: Discrete schemes for Gaussian curvature and their convergence. Comput. Math. Appl. **57**(7), 1187–1195 (2009)
87. Zhang, L., Razdan, A., Farin, G., Femiani, J., Bae, M., Lockwood, C.: 3D face authentication and recognition based on bilateral symmetry analysis. Vis. Comput. **22**(1), 43–55 (2006)

Yinhang Tang received the B.S. degree in mathematics and applied mathematics and the M.S. degree in computer science from Beihang University, Beijing, China, in 2010 and 2013 respectively. He also obtained the degree of general engineering from Ecole Centrale de Pekin, Beijing, China, in 2013. He is currently working toward the Ph.D degree in computer vision with LIRIS, Ecole Centrale de Lyon, Lyon, France. His current research interests include 3D face analysis, image processing, spoofing attack and hand vein recognition.

Huibin Li received the B.S. degree in mathematics from Shaanxi Normal University, Xi'an, China, in 2006, the M.S. degree in mathematics from Xi'an Jiatong University, Xi'an, China, in 2009, and the Ph.D. degree in computer science from Ecole Centrale de Lyon, Lyon, France, in 2013. Then he jointed the Institute from Information and System Sciences, School of Mathematics and Statistics, Xi'an Jiaotong University. His current research interests include generalized curvatures, computational conformal mapping, 3D facial expression recognition, 3D face recognition, and deep learning for 3D shape analysis.

Xiang Sun received his Ph.D. from King Abdullah University of Science and Technology, Thuwal, Saudi Arabia. Main interests: Discrete differential geometry, in particular discrete curvature theories and their applications to different elds such as computer graphics, geometric modelling, free-form architectural design, face recognition.

Jean-Marie Morvan received the Ph.D. from the University Paul Sabatier, Toulouse, France. He is a professor of mathematics with the University Claude Bernard Lyon 1, Lyon, France, and a Visiting Professeur at the King Abdullah University of Science and Technology (KAUST), Thuwal, Saudi Arabia. His research interests include differential geometry, in particular Riemannian and symplectic geometry, geometric measure theory, and application of geometry to different fields, such as geology, geophysics, computer graphics, and algorithmic geometry.

Liming Chen received the joint B.Sc. degree in mathematics and computer science from the University of Nantes in 1984, and the M.S. and Ph.D. degrees in computer science from the University of Paris 6 in 1986 and 1989, respectively. He first served as an associate professor at the Université de Technologie de Compiègne, and then joined Ecole Centrale de Lyon (ECL) as a professor in 1998, where he leads an advanced research team in multimedia computing and pattern recognition. He has been the head of the Department of Mathematics and Computer Science at ECL since 2007. His current research interests include computer vision and multimedia, in particular 2D/3D face analysis, image and video categorization, and affective computing.